ARTICLE

doi:10.1038/nature13442

Topoisomerase II mediates meiotic crossover interference

Liangran Zhang[1], Shunxin Wang[1], Shen Yin[1], Soogil Hong[2], Keun P. Kim[2] & Nancy Kleckner[1]

Spatial patterning is a ubiquitous feature of biological systems. Meiotic crossovers provide an interesting example, defined by the classic phenomenon of crossover interference. Here we identify a molecular pathway for interference by analysing crossover patterns in budding yeast. Topoisomerase II plays a central role, thus identifying a new function for this critical molecule. SUMOylation (of topoisomerase II and axis component Red1) and ubiquitin–mediated removal of SUMOylated proteins are also required. The findings support the hypothesis that crossover interference involves accumulation, relief and redistribution of mechanical stress along the protein/DNA meshwork of meiotic chromosome axes, with topoisomerase II required to adjust spatial relationships among DNA segments.

During meiosis, crossovers promote genetic diversity and create physical connections between homologues that ensure their accurate segregation (reviewed in refs 1–3). Crossovers arise stochastically from a larger set of undifferentiated precursor recombination complexes, having different positions in different nuclei. Nonetheless, along any given chromosome in any given nucleus, crossovers tend to be evenly spaced (reviewed in refs 3 and 4). This genetic phenomenon is termed crossover interference[5,6].

Crossover interference implies the occurrence of communication along chromosomes, over distances ranging from 300 nm to more than 30 μm (refs 4, 7 and 8). Some models for crossover interference invoke spreading of a molecular-based change along the chromosomes[9]. Even spacing can also be achieved by a reaction–diffusion process[10]. We have proposed, alternatively, that interference involves the accumulation, relief and redistribution of mechanical stress, with spreading molecular changes following as a consequence of spreading stress relief[4]. Aberrant crossover patterns are observed in mutants defective for recombination, chromosome structure, chromatin state and DNA-based signal transduction. However, no specific molecular process has been defined. To address this deficit, we examined crossover patterns in wild-type (WT) and mutant strains of budding yeast as defined by cytological localization of crossover-correlated molecular foci.

Crossover interference in WT meiosis

Mammals, plants and fungi share a common meiotic recombination program. Recombination initiates by programmed double-strand breaks (DSBs), which occur as chromosome structural axes develop[11,12]. Each DSB identifies its homologous partner duplex and mediates whole chromosome pairing. As a result, homologue structural axes are co-aligned, linked by bridging recombination complexes[13]. Crossover patterning is thought to act upon these bridging interactions[13,14], designating a subset to be crossovers, with accompanying interference[14,15]. In yeast, crossover designation locally nucleates formation of synaptonemal complex between homologue axes[13,14,16]. Synaptonemal complex then spreads along the lengths of the chromosomes. Correspondingly, crossover patterning and interference are independent of synaptonemal complex formation[13,17,18] (below).

In yeast, foci of E3 ligase Zip3, which specifically mark the sites of patterned crossovers[8,18–20], serve as an early marker for crossover interference analysis (Methods). Zip3 foci emerge immediately following crossover designation, thus avoiding complications arising during formation of actual crossover products[8]. Also, Zip3 foci do not mark the sites of additional crossovers that arise by other routes[8] (Methods).

Zip3-MYC foci were visualized along synaptonemal complexes of surface-spread pachytene chromosomes by wide-field epifluorescence[8] (Fig. 1a, b). Each Zip3 focus position was defined, to an accuracy of approximately one pixel (67 nm) along a particular marked chromosome in ~200–300 nuclei, thus defining patterns with a high degree of reproducibility and accuracy[8] (Supplementary Table 1). Using these position data, the distance along a chromosome over which the interference signal is detectable (that is, the 'interference distance', L) is defined by three different approaches (Fig. 1c–e). In each case, L is given in units of physical distance (rationale below), micrometres of synaptonemal complex, which is a proxy for chromosome length at late leptotene when crossover designation actually occurs (above).

Crossover interference is classically described by coefficient of coincidence (CoC) analysis[5,6,8] (Fig. 1c; see Methods). Zip3 foci along three chromosomes of different sizes (330–1,530 kilobases (kb)) exhibit classic coefficient of coincidence relationships (Fig. 1d, left column). For intervals that are close together, bivalents exhibiting a focus in each interval ('double events') are much rarer than expected, reflecting operation of interference; as the inter-interval distance increases, double-event frequencies progressively approach, then reach, that expected for independent occurrence, where the observed frequency is the same as the expected frequency (coefficient of coincidence = 1). At even longer intervals, coefficient of coincidence values can exceed 1, reflecting the tendency for even spacing[8]. For convenience, we define the interference distance described by such curves as the inter-interval distance at which the coefficient of coincidence = 0.5, namely L_{CoC} (Fig. 1d, left column). The three analysed chromosomes exhibit virtually identical coefficient of coincidence curves and values of $L_{CoC} = 0.3 \pm 0.01$ μm[8] ($n = 2$–4; Fig. 1d, left column; Methods).

We previously described a stress-and-stress relief mechanism for crossover patterning (the 'beam-film' (BF) model). Beam-film-predicted crossover patterns are defined by simulation analyses[8] that can accurately describe crossover patterns in diverse organisms, including yeast (Fig. 1d, middle and right columns). The beam-film parameter (L) is the distance over which the interference signal spreads along the chromosomes and corresponds to the distance at which the predicted coefficient of coincidence = 0.5, namely L_{BF}. Beam-film simulations give the same value of L and $L_{BF} \approx 0.3$ μm for all three analysed yeast chromosomes (Fig. 1d, middle column).

[1]Department of Molecular and Cellular Biology, Harvard University, Cambridge, Massachusetts 02138, USA. [2]Department of Life Science, Chung-Ang University, Seoul 156-756, South Korea.

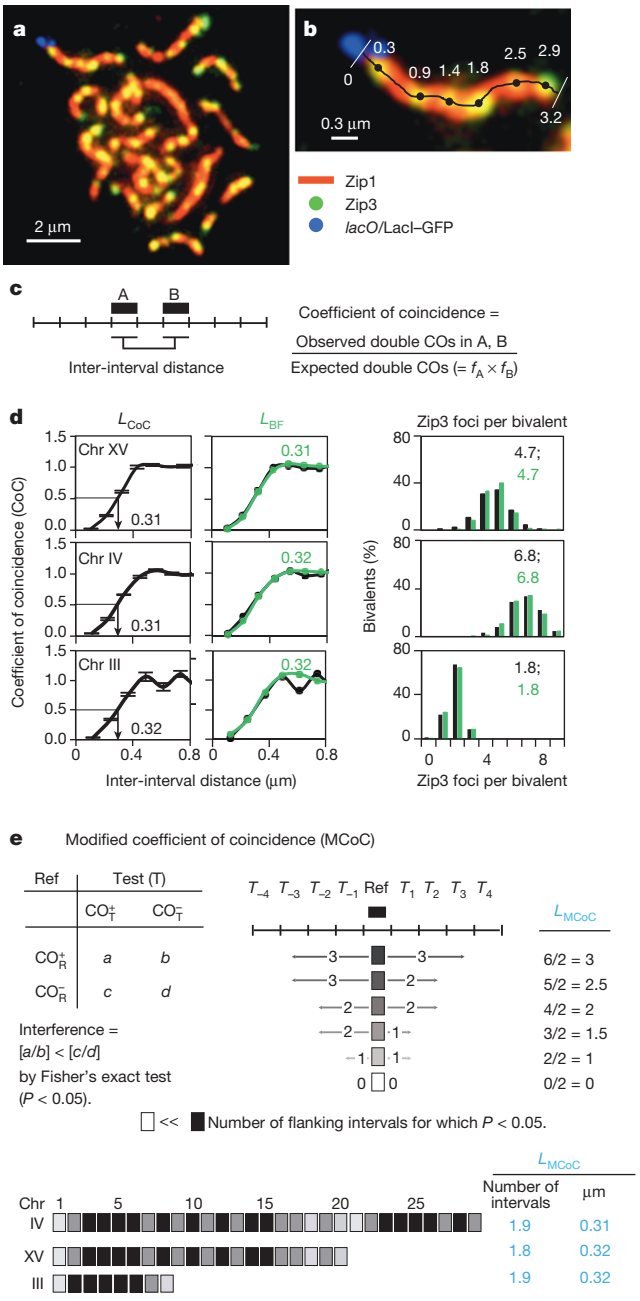

Figure 1 | Crossover interference in WT meiosis. **a**, Spread yeast pachytene chromosomes labelled for synaptonemal complex component Zip1 (red), crossover-correlated Zip3 foci (green) and a *lacO*/LacI–GFP (green fluorescent protein) array at the end of chromosome XV (blue). **b**, Positions of Zip3 foci along a chromosome XV bivalent and total synaptonemal complex were determined in a single continuous trace. **c**, Definition of coefficient of coincidence. CO, crossover. **d**, Coefficient of coincidence and average number/distribution of crossovers on chromosomes (Chr) XV, III and IV (black). Bars, s.e.m. Beam-film best-fit simulations in green. L_{CoC} and $L_{BF} = 0.3 \pm 0.01$ μm for all three chromosomes ($n = 4$, 3 and 2 experiments, 200–300 bivalents each). **e**, Modified coefficient of coincidence analysis defines, for each interval, the number of adjacent intervals affected by crossover interference. Top left: each interval is considered individually as a reference interval (Ref). Chromosomes that do or do not contain a crossover in that interval (CO^+_R, CO^-_R) are evaluated for the number that do or do not contain a crossover in a second (nearby) interval (Test; CO^+_T, CO^-_T). Fisher's exact test is applied to determine whether there were fewer crossovers in the CO^+_R group versus the CO^-_R group, implying interference emanating from the reference interval to the test interval. Top right: number of nearby test intervals where interference was detected in one direction from the reference interval gives L_{MCoC} for that interval. Bottom: average L_{MCoC} for all reference intervals along a chromosome (0.16 μm per interval): $L_{MCoC} \approx 0.3$ μm for all three chromosomes (Extended Data Fig. 3a).

Crossover interference can be examined by a modified coefficient of coincidence analysis (MCoC[21], Fig. 1e; Methods). The three analysed yeast chromosomes exhibit the same average L_{MCoC} of ~0.3 μm.

Crossover interference requires topoisomerase II

Topoisomerase II (TopoII) alleviates topological stresses within chromosomes. If crossover interference involves mechanical stress along the chromosomes[4], TopoII could be a key player. We assessed crossover interference in three mutants with altered TopoII states (Fig. 2 and Extended Data Figs 1–3). (1) TopoII was depleted using a *pCLB2-TOP2* fusion that expressed TopoII in vegetative cells but not meiosis. (2) TopoII catalytic activity was eliminated in meiosis by expressing a catalytically inactive allele (*top2YF*) under its native promoter in a *pCLB2-TOP2* strain, leaving *top2YF* as the only gene expressed during meiosis. (3) SUMOylation of TopoII at several carboxy (C)-terminal residues[22] was eliminated by mutation. All three *top2* mutant strains grow well vegetatively, progress to the pachytene stage of meiosis and exhibit normal synaptonemal complex morphology and length[23] (Extended Data Fig. 3). Meiotic TopoII levels and localization were severely reduced in *pCLB2-TOP2* and not detectably changed in other mutants (Extended Data Fig. 1).

In all three *top2* mutant strains, for all three analysed chromosomes, the interference distance as defined by L_{CoC}, L_{BF} and L_{MCoC} decreased from ~0.3 μm in WT to ~0.2 μm (Fig. 2a, b and Extended Data Figs 2 and 3). Reduced interference should be accompanied by an increased number of crossovers, and, in all cases, the distribution of Zip3 foci per bivalent was shifted to higher values (Fig. 2a, b and Extended Data Fig. 2).

For *pCLB2-TOP2*, the interference defect was confirmed by a fourth approach. Meiotic crossover patterns are characterized by 'crossover homeostasis'[24]. A decrease or increase in the frequency of DSBs (and thus crossover precursor interactions) necessarily changes the crossover frequency. However, the magnitudes of such changes are less than proportional to the change in DSB/precursor frequency, implying a homeostatic effect. Crossover homeostasis is a direct consequence of crossover interference[8,24]: homeostatic disparity is greater or less when crossover interference is stronger or weaker, and absent when crossover interference is absent. This interplay is predicted, and can be quantified, by beam-film simulations[8] (Fig. 2d).

To evaluate crossover homeostasis experimentally, the number of Zip3 foci along a given chromosome was determined in a series of strains that exhibited different levels of DSBs (precursors). Decreased and increased levels are conferred by hypomorphic mutations in DSB transesterase Spo11 and a *tel1Δ* mutation respectively[8] (Extended Data Fig. 4 and Fig. 2d). In a *TOP2* background, homeostasis is apparent in the nonlinear relationship of Zip3 focus number to DSB number (chromosomes XV and III; Fig. 2d, filled black circles, and Extended Data Fig. 4)[8]. Moreover, the experimentally defined relationships occur at exactly the level of interference predicted to occur in WT meiosis by best-fit beam-film simulation analysis[8] ($L_{BF} \approx 0.3$ μm; above; Fig. 2d).

If *pCLB2-TOP2* reduces the interference distance, it should bring the relationship between Zip3 focus number and DSB number closer to the linear proportionality seen in the absence of interference. This prediction is fulfilled (chromosomes XV and III; Fig. 2d filled pink circles and Extended Data Fig. 4). Furthermore, the mutant relationships again occur specifically at the interference distance predicted by best-fit beam-film simulation analysis for this mutant ($L_{BF} \approx 0.2$ μm; Fig. 2d and Extended Data Fig. 4). These results confirm the existence of an interference defect in *pCLB2-TOP2* and provide further evidence that the beam-film model can accurately describe crossover patterns (see also Extended Data Fig. 4).

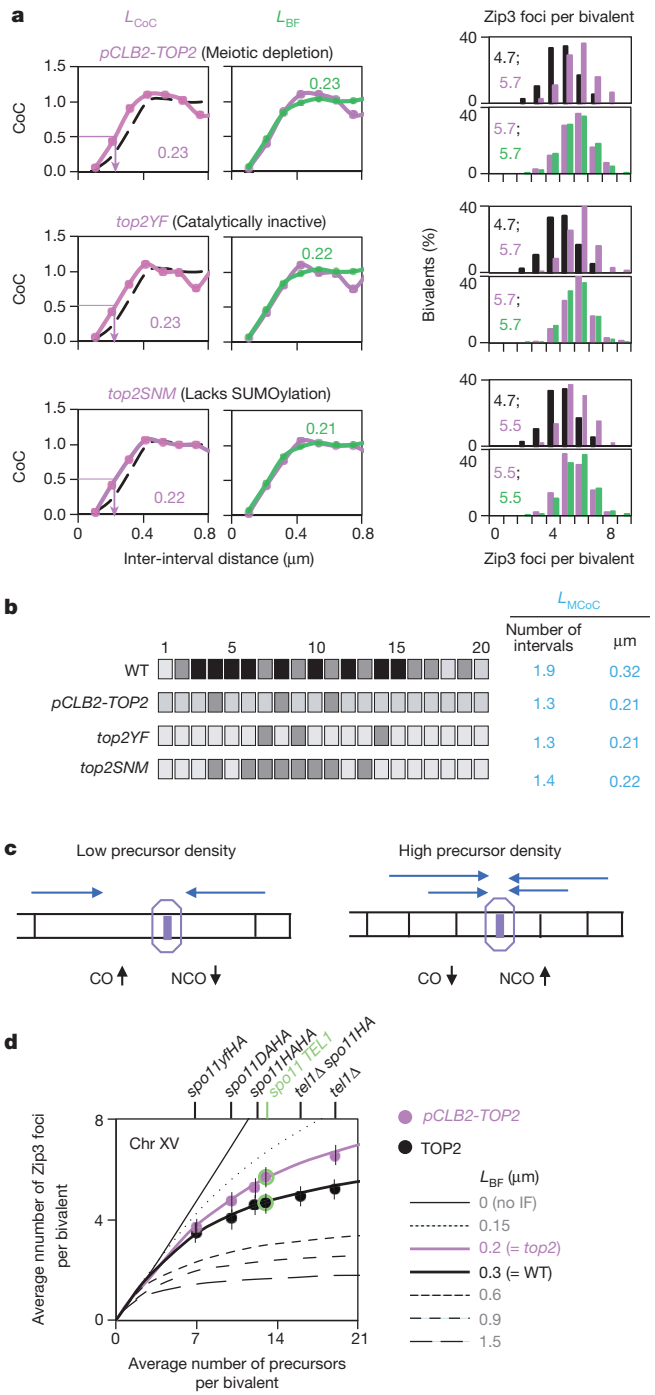

Figure 2 | Crossover interference in *top2* mutants. **a**, **b**, All three *top2* mutants show decreased crossover interference by all criteria (L_{CoC}, L_{BF}, L_{MCoC}) and correspondingly increased crossover frequency. **a**, WT, *top2* and beam-film (BF) simulation data (black, pink and green). **c**, The basis for crossover homeostasis[8]. CO, crossover; NCO, non-crossover. At lower (higher) precursor density (black vertical lines; left (right)), a given precursor will be less (more) likely to experience interference emanating from nearby crossovers (indicated by fewer (more) blue lines), giving an increased (decreased) probability of a crossover at each individual position, and thus along the whole chromosome length. The magnitudes of these effects will be greater or lesser according to the strength of crossover interference (and zero in its absence). **d**, Quantitative evaluation of crossover homeostasis on chromosome XV. Lines: relationship of crossover number to precursor number (parameter *N*) predicted by beam-film simulations at varying interference levels (L_{BF} = interference distance, *L*; other parameters appropriate to WT yeast meiosis[8]). Crossover homeostasis decreases with decreasing crossover interference. Filled circles: strains exhibiting altered DSB levels (top) were analysed for Zip3 foci in *TOP2* (black) and *pCLB2-TOP2* (pink) backgrounds (Extended Data Fig. 4). Average frequency of Zip3 foci per bivalent plotted versus DSB (= precursor) number (vertical lines indicate s.d.). *pCLB2-TOP2* differs experimentally from WT in the direction expected for decreased crossover interference. Experimental data for WT and *pCLB2-TOP2* both quantitatively match the relationships predicted for their corresponding interference levels by beam-film simulations (L_{BF} = 0.3 and 0.2 μm, respectively; Fig. 2a, b).

Crossover interference requires SUMO and STUbL

SUMOylation of TopoII requires Ubc9, the only known SUMO–E2 of yeast[25]. Another Ubc9 substrate is meiotic axis component Red1 (ref. 20). Mutation of the SUMOylation patch of Red1, which dramatically reduces the level of modification (*red1KR*[26]), confers the same altered Zip3 focus patterns as *top2* mutations, including *top2SNM* (Fig. 3a and Extended Data Fig. 3). Interestingly the non-null allele, *ubc9–GFP*[27], also exhibits this phenotype (Fig. 3a and Extended Data Fig. 3), as well as an elevated level of crossovers as defined genetically[27].

Crossover interference also requires STUbL protein Slx5/8. Slx5/8 ubiquitinates SUMOylated proteins, targeting them for removal from their cognate complexes[28]. Absence of Slx5/8 activity confers a strong global increase in protein SUMOylation during meiosis (Extended Data Fig. 5). Absence of either Slx5 or Slx8, or mutational abrogation of either the Slx5 SUMO-binding motif or the Slx8 ubiquitin ligase motif (*slx5Δ*, *slx8Δ*, *slx5-SIM* or *slx8-SS*), confers the same changes in Zip3 focus patterns as *top2*, *red1-KR* and *ubc9–GFP* (Fig. 3b and Extended Data Figs 2 and 3). The *slx5Δ* defect is confirmed genetically (Extended Data Fig. 3 and Supplementary Table 2).

The sirtuin, Sir2, enables Slx5/8 STUbL activity[29] and is required for crossover interference via that activity. The absence of Sir2 (*sir2Δ*) or specific elimination of the interaction of Sir2 with Slx5/8 (*sir2RK*) confer the same changes in Zip3 focus patterns as all of the other mutations analysed above, by all criteria (Fig. 3c and Extended Data Figs 2 and 3). The interference defect in *sir2RK* was confirmed genetically (Extended Data Fig. 3 and Supplementary Table 2).

The role of Sir2 in interference is specific to this one function. Elimination of other Sir2-mediated activities (histone deacetylase catalysis (*sir2-345*); interaction with Sir2 partners required for silencing (deletion mutants of Sir3, Sir4, Esc2 and Esc8); cohesion (*sir2ΔC500*)) does not alter crossover interference (Fig. 3c and Extended Data Figs 3 and 6).

A single TopoII crossover interference pathway

Not only do all analysed mutants exhibit the same quantitative defects in crossover interference and crossover number as defined by Zip3 focus patterns (Figs 2–4 and Extended Data Figs 2 and 3), but double mutants carrying combinations of single mutations also exhibit these same phenotypes (Fig. 4a,b). Thus, the described mutants define a single molecular pathway.

This pathway may directly implement the spreading interference signal, but other perturbations are not excluded (Supplementary Discussion). These results cannot be explained by (1) prolongation of the crossover-designation period, (2) higher DSB/precursor levels (Extended Data Figs 4, 7 and 8) or (3) obviously altered axis organization, since all mutants exhibit WT synaptonemal complex lengths (Extended Data Fig. 3). All mutants exhibit reduced evenness of spacing as defined by gamma distribution analysis (Supplementary Discussion).

The obligatory crossover does not require interference

Since a crossover is required for meiotic homologue segregation, every pair of homologues must acquire at least one (the 'obligatory crossover')[3]. The frequency of zero-Zip3 focus chromosomes is less than 10^{-3} for chromosomes IV and XV and ~1% for chromosome III because it is small[8]. None of the identified interference-defective mutants exhibits an increased frequency of zero-Zip3 foci chromosomes (Figs 1–4 and

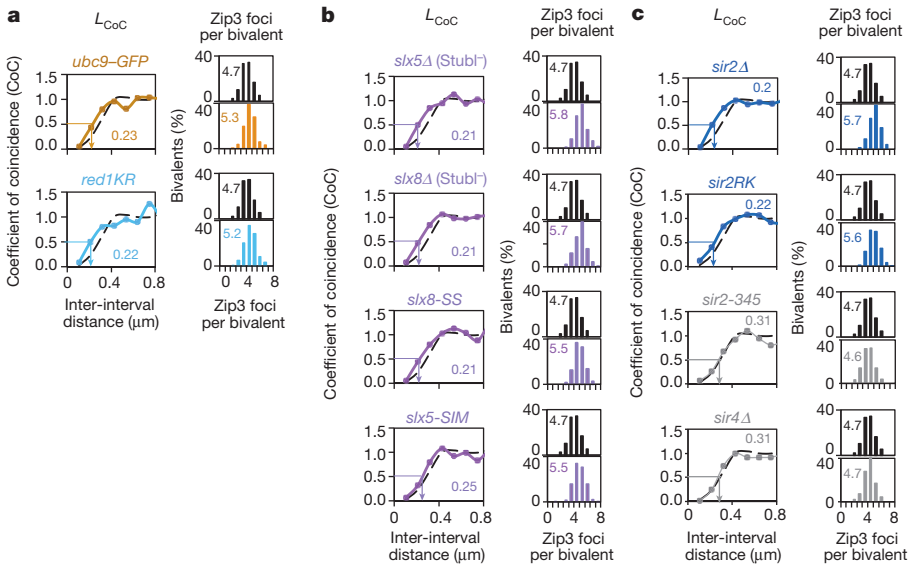

Figure 3 | Crossover interference requires post-translational modification. **a–c**, WT and mutant crossover patterns (black; colours). Quantitatively similar decreases in crossover interference and increases in crossover number are seen in *ubc9–GFP* (SUMO E2; brown), *red1KR* (non-SUMOylated Red1; cyan), strains lacking Slx5 or Slx8 (*slx5Δ* or *slx8Δ*) or mutated for the Slx5 SUMO-binding motif or the Slx8 ubiquitin ligase motif (*slx5-SIM*, *slx8-SS*) (magenta), or lacking Sir2 (*sir2Δ*) or mutated for the Sir2/Slx5 interaction site (*sir2RK*) (blue). Crossover interference does not require Sir2 deacetylation activity (*sir2-345*), Sir2 interaction partner Sir4 (*sir4Δ*) (grey) or other Sir2 activities/partners (text).

Extended Data Fig. 2). This result argues against models in which crossover interference is required to ensure the obligatory crossover[8,9] whereas the beam-film model predicts this phenotype[8].

The crossover interference metric is physical distance

We analysed Zip3 focus patterns in strains whose pachytene synaptonemal complex lengths differ from those of the reference WT SK1 strain (Fig. 5 and Extended Data Fig. 9). These strains exhibit different interference distances when the metric used is genomic length (kilobases) but exactly the same (WT) interference distance when the metric is physical length as micrometres of synaptonemal complex (Fig. 5; compare top and bottom panels). Beam-film simulations give the same relationships (Extended Data Fig. 9a–c). Thus, in budding yeast, the metric for spreading crossover interference is physical chromosome distance, as in mouse, *Arabidopsis*, human and tomato[8,30–32]. Differences in synaptonemal complex length probably result from altered chromatin loop lengths (kilobases) without a change in basic axis structure[33,34]. In all cases, experimental Zip3 focus distributions are matched by beam-film simulations that use the WT value for interference distance (L_{BF}). These and other details (Extended Data Fig. 9 legend) provide further evidence of the precision with which the beam-film model explains diverse crossover patterns.

The TopoII interference pathway is highly specific

None of more than 20 other examined mutants exhibit altered Zip3 focus patterns, including those with the following: (1) altered axis composition (condensin, *pch2Δ*); (2) lacking either a sister chromatid (*cdc6*) or any/normal synaptonemal complex (*zip1Δ*; *msh4Δ*)[8,18] (Fig. 5; discussion in Extended Data Fig. 9a and Methods); or (3) deleted for Sir2 relative, Hst1; ATM homologue Tel1; meiotic telomere/motion protein Ndj1; chromodomain protein Dot1; DSB-triggered γ-H2A; TopoII-colocalizing Nse1/Smc5/6; nucleosome density factor Yta7; Mph1, Mlh1/3 and Mms4 (recombination resolution); or Msh2 (mismatch repair) (Extended Data Fig. 6; L.Z., unpublished observations).

Discussion

Our findings show that Topoisomerase II is essential for normal CO interference. Further, crossover interference is mediated by communication along prophase chromosome structural axes (Fig. 6a). The TopoII interference pathway involves SUMOylation of Red1, a prominent meiotic axis component. TopoII itself occurs prominently along meiotic prophase axes, in yeast and mammals[35,36] and along the structural axes of mammalian mitotic late-stage chromosomes, to which meiotic axes are related[37]. Moreover, the TopoII interference pathway requires SUMOylation of TopoII as well as Red1. In mitotic mammalian cells, SUMOylated TopoII is implicated in late-stage chromosome structural axes[38], and in yeast, SUMOylated TopoII occurs preferentially in centromere regions[39] which, during meiosis, mimic crossover-designation/interference sites by nucleating synaptonemal complex formation[16]. Spreading of interference along the axis matches our finding that the relevant metric is physical chromosome distance and the inference that variations in synaptonemal complex length in different mutants result from variations in loop length rather than basic axis structure. Finally, spreading along the axis explains how the interference signal is first generated by, then sensed by, biochemical recombination complexes, which are intimately embedded in the axes from their first inception as pre-DSB ensembles[12]. Notably, the meiotic prophase axis probably comprises a meshwork of DNA segments joined by linker proteins[1,33,37] (Fig. 6a, b).

Most importantly, crossover interference requires the catalytic activity of TopoII. Since TopoII activity does not require input of external energy from ATP hydrolysis, its reactions must be driven forward, and given directionality, by their substrates, which are changed by TopoII from a higher potential energy state to a lower potential energy state. If substrate for TopoII during crossover interference is the axis meshwork (above), that meshwork is first placed in a high potential energy state and then, in response to crossover designation, undergoes relaxation, dependent upon TopoII activity. That is, the axis meshwork begins in a mechanically stressed state and is then relaxed to a less mechanically stressed state dependent upon TopoII. This progression closely matches the proposed stress and stress relief mechanism for crossover patterning[4,14] (Methods): stress accumulates along the chromosomes and provokes local crossover designation which, by its intrinsic nature, results in local relief of stress. That local change then redistributes along the chromosomes, emanating outwards from its nucleation site, reducing stress and thereby disfavouring additional stress-promoted crossover designations in the affected regions.

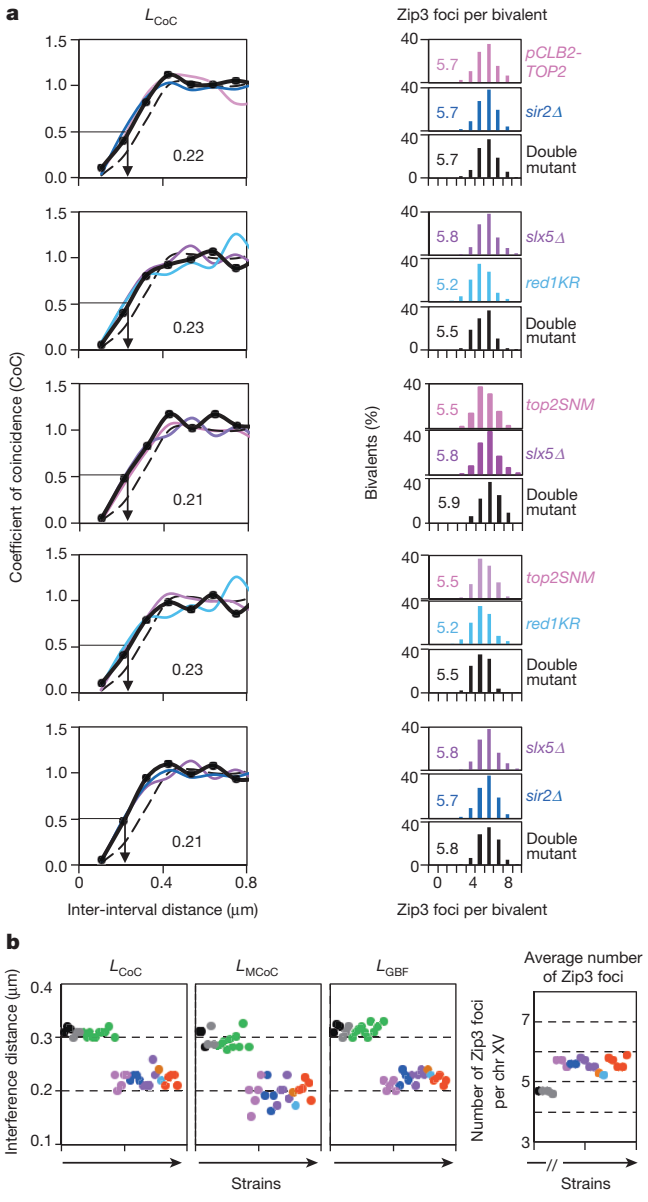

Figure 4 | A single pathway for crossover interference. **a**, Representative double mutants and component single mutants exhibit the same quantitative defect in crossover interference and increased crossover number (colours and black) versus WT (dashed line). **b**, Crossover interference and crossover number phenotypes for all mutants (Figs 1–5). WT (black), *sir2-345* and *sir4Δ* (grey), *top2* mutants (pink), *sir2Δ* and *sir2RK* (blue), *slx5/8* mutants (purple), *ubc9–GFP* (brown), *red1KR* (light blue), double mutants (red); mutants with altered axis length showing WT phenotype (green).

In this context, what is the source of meshwork stress and how does TopoII alleviate that stress? We previously suggested that mechanical stress arises from axis-constrained global chromatin expansion; crossover designation and interference then involve local nucleation and spreading of chromatin/axis compaction[4,14] (Fig. 6b). TopoII could act during compaction to adjust spatial relationships among DNA segments within the axis meshwork (Fig. 6b), thereby implementing both local relief of stress and its redistribution. The stress-relief role of TopoII is thus specifically targeted to the compaction process, and thus to regions undergoing crossover designation/interference. This role also explains why the TopoII pathway is important, but not absolutely essential, for crossover interference: in its absence, the basic process of spreading stress relief would occur, but full relaxation would not be possible without meshwork readjustment (Fig. 6b). Interestingly, mitotic chromosomes are constrained by topologically sensitive linkages and collapse upon removal of protein/DNA links[40,41], exactly as expected for a meshwork under expansion stress.

We further note that the beam-film model, formulated to quantitatively describe the predictions of a stress and stress-relief mechanism[4,8], accurately and quantitatively describes diverse crossover patterning data for WT meiosis, including crossover homeostasis, in yeast and other organisms[8] (Figs 1d and 2d), as well as crossover patterning in mutants. These include the following: (1) crossover interference, crossover number and crossover homeostasis in mutants defective in the TopoII interference pathway (Fig. 2a, d; not shown); (2) crossover patterns at varying DSB levels in those mutants (Extended Data Fig. 4); and (3) crossover patterns in mutants with altered axis lengths (Extended Data Fig. 9a, b). Recent findings in *Caenorhabditis elegans*[42] can also be directly explained by such a model (Supplementary Discussion). Importantly, however, the mathematical formulation of the beam-film model can equivalently describe any mechanism involving progressive 'event designation' and resulting interference that decays exponentially away from the designation site. Thus, proof that crossover patterning involves macroscopic mechanical effects requires direct identification of such effects.

Finally, our results implicate SUMOylation (of Red1 and TopoII, probably among multiple targets) and ubiquitin-targeted removal of SUMOylated proteins in the TopoII crossover interference pathway. These effects presumably act sequentially on the same molecules, which are first specifically SUMOylated and then targeted for removal via STUbL activity. SUMOylation might establish preconditions for crossover interference whose subsequent implementation would require removal of those SUMOylated proteins. Alternatively, SUMOylation and STUbL activity might compete actively in a single aspect of the patterning process; or SUMOylation might function only to target protein removal. For yeast TopoII, absence of SUMOylation (in *top2SNM*) decreases the mobility of chromosome-bound TopoII[43], perhaps promoting repeated cycles of TopoII catalytic activity.

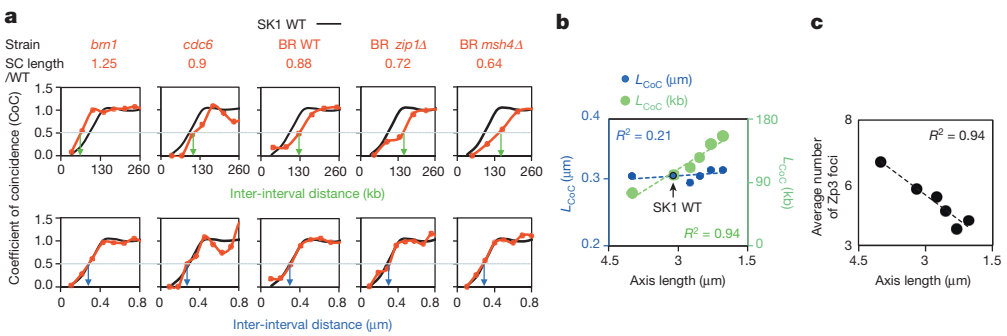

Figure 5 | The metric of crossover interference is physical chromosomal length (micrometres). **a**, **b**, Coefficient of coincidence relationships for strains with different axis lengths (red) relative to WT SK1 (black). **a**, Interference lengths differ in genomic distance (kilobases) (top) but are the same in physical distance (micrometres of synaptonemal complex (SC)) (bottom). **b**, L_{CoC} values from **a** with corresponding linear regression lines. **c**, Zip3 focus frequencies vary linearly with bivalent axis/synaptonemal complex length.

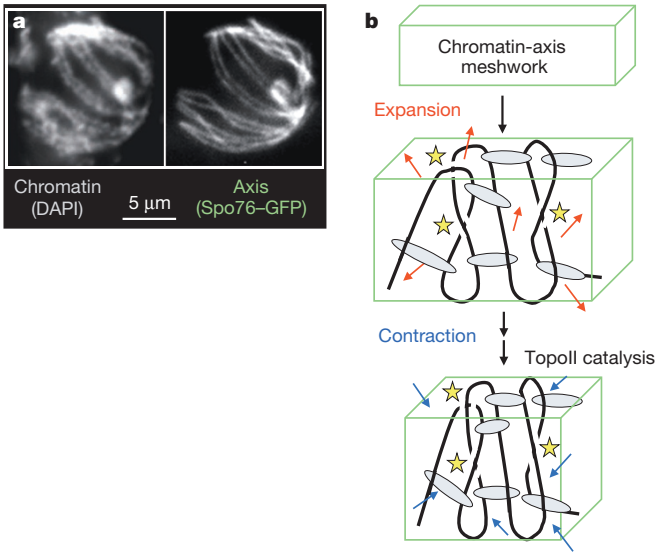

Figure 6 | Proposed role of TopoII for crossover interference. **a**, Chromosomes at the crossover-designation stage (late leptotene), visualized in Sordaria, suggest that the axis (identified with Spo76–GFP) incorporates a significant fraction of chromatin (stained with DAPI) in a DNA/protein structural meshwork. **b**, Model. Top: global chromatin expansion within the structural axis meshwork is constrained by meshwork tethers, giving an expanded, mechanically stressed meshwork state. Bottom: spreading interference creates a more contracted state with resulting reduction in mechanical meshwork stress. Full implementation of contraction, and thus maximal spreading of interference, requires readjustment of spatial relationships among component DNA segments which, comprising topologically closed domains, require TopoII-mediated duplex/duplex passages (yellow stars).

METHODS SUMMARY

Analysed yeast strains were isogenic SK1 derivatives (Extended Data Table 1). Details of analyses are described in ref. 8, Methods and Extended Data. Zip3 focus positions and synaptonemal complex lengths for all experiments are in Supplementary Table 1. Data for BR strains (Fig. 5) were provided by J. Fung.

Online Content Methods, along with any additional Extended Data display items and Source Data, are available in the online version of the paper; references unique to these sections appear only in the online paper.

Received 19 November 2013; accepted 2 May 2014.
Published online 13 July 2014.

1. Kleckner, N., Zhang, L., Weiner, B. & Zickler, D. in *Genome Organization and Function in the Cell Nucleus* (ed. Rippe, K.) 487–533 (John Wiley, 2011).
2. Zickler, D. & Kleckner, N. The leptotene-zygotene transition of meiosis. *Annu. Rev. Genet.* **32,** 619–697 (1998).
3. Jones, G. H. & Franklin, F. C. Meiotic crossing-over: obligation and interference. *Cell* **126,** 246–248 (2006).
4. Kleckner, N. *et al.* A mechanical basis for chromosome function. *Proc. Natl Acad. Sci. USA* **101,** 12592–12597 (2004).
5. Muller, H. J. The mechanism of crossing over, parts I–IV. *Am. Nat.* **50,** 193–434 (1916).
6. Sturtevant, A. H. The behavior of the chromosomes as studied through linkage. *Z. indukt. Abstamm.-u. VererbLehre* **13,** 234–287 (1915).
7. Hillers, K. J. & Villeneuve, A. M. Chromosome-wide control of meiotic crossing over in *C. elegans*. *Curr. Biol.* **13,** 1641–1647 (2003).
8. Zhang, L., Liang, Z., Hutchinson, J. & Kleckner, N. Crossover patterning by the Beam-Film model: analysis and implications. *PLoS Genet.* **10,** e1004042 (2014).
9. King, J. S. & Mortimer, R. K. A polymerization model of chiasma interference and corresponding computer simulation. *Genetics* **126,** 1127–1138 (1990).
10. Vecchiarelli, A. G., Hwang, L. C. & Mizuuchi, K. Cell-free study of F plasmid partition provides evidence for cargo transport by a diffusion-ratchet mechanism. *Proc. Natl Acad. Sci. USA* **110,** E1390–E1397 (2013).
11. Blat, Y., Protacio, R. U., Hunter, N. & Kleckner, N. Physical and functional interactions among basic chromosome organizational features govern early steps of meiotic chiasma formation. *Cell* **111,** 791–802 (2002).
12. Pan, J. *et al.* A hierarchical combination of factors shapes the genome-wide topography of yeast meiotic recombination initiation. *Cell* **144,** 719–731 (2011).
13. Storlazzi, A. *et al.* Recombination proteins mediate meiotic spatial chromosome organization and pairing. *Cell* **141,** 94–106 (2010).
14. Borner, G. V., Kleckner, N. & Hunter, N. Crossover/noncrossover differentiation, synaptonemal complex formation, and regulatory surveillance at the leptotene/zygotene transition of meiosis. *Cell* **117,** 29–45 (2004).
15. Hunter, N. in *Molecular Genetics of Recombination, Topics in Current Genetics* (eds Aguilera, A. and Rothstein, R.) 381–442 (Springer, 2006).
16. Henderson, K. A. & Keeney, S. Synaptonemal complex formation: where does it start? *Bioessays* **27,** 995–998 (2005).
17. Bishop, D. K. & Zickler, D. Early decision; meiotic crossover interference prior to stable strand exchange and synapsis. *Cell* **117,** 9–15 (2004).
18. Fung, J. C., Rockmill, B., Odell, M. & Roeder, G. S. Imposition of crossover interference through the nonrandom distribution of synapsis initiation complexes. *Cell* **116,** 795–802 (2004).
19. Agarwal, S. & Roeder, G. S. Zip3 provides a link between recombination enzymes and synaptonemal complex proteins. *Cell* **102,** 245–255 (2000).
20. Cheng, C. H. *et al.* SUMO modifications control assembly of synaptonemal complex and polycomplex in meiosis of *Saccharomyces cerevisiae*. *Genes Dev.* **20,** 2067–2081 (2006).
21. Malkova, A. *et al.* Gene conversion and crossing over along the 405-kb left arm of *Saccharomyces cerevisiae* chromosome VII. *Genetics* **168,** 49–63 (2004).
22. Bachant, J., Alcasabas, A., Blat, Y., Kleckner, N. & Elledge, S. J. The SUMO-1 isopeptidase Smt4 is linked to centromeric cohesion through SUMO-1 modification of DNA topoisomerase II. *Mol. Cell* **9,** 1169–1182 (2002).
23. Rose, D. & Holm, C. Meiosis-specific arrest revealed in DNA topoisomerase II mutants. *Mol. Cell. Biol.* **13,** 3445–3455 (1993).
24. Martini, E., Diaz, R. L., Hunter, N. & Keeney, S. Crossover homeostasis in yeast meiosis. *Cell* **126,** 285–295 (2006).
25. Baldwin, M. & Bachant, J. Top2 SUMO conjugation in yeast cell lysates. *Methods Mol. Biol.* **582,** 209–219 (2009).
26. Eichinger, C. S. & Jentsch, S. Synaptonemal complex formation and meiotic checkpoint signaling are linked to the lateral element protein Red1. *Proc. Natl Acad. Sci. USA* **107,** 11370–11375 (2010).
27. Hooker, G. W. & Roeder, G. S. A Role for SUMO in meiotic chromosome synapsis. *Curr. Biol.* **16,** 1238–1243 (2006).
28. Nagai, S., Davoodi, N. & Gasser, S. M. Nuclear organization in genome stability: SUMO connections. *Cell Res.* **21,** 474–485 (2011).
29. Darst, R. P., Garcia, S. N., Koch, M. R. & Pillus, L. Slx5 promotes transcriptional silencing and is required for robust growth in the absence of Sir2. *Mol. Cell. Biol.* **28,** 1361–1372 (2008).
30. Drouaud, J. *et al.* Sex-specific crossover distributions and variations in interference level along *Arabidopsis thaliana* chromosome 4. *PLoS Genet.* **3,** e106 (2007).
31. Petkov, P. M., Broman, K. W., Szatkiewicz, J. P. & Paigen, K. Crossover interference underlies sex differences in recombination rates. *Trends Genet.* **23,** 539–542 (2007).
32. Hou, Y. *et al.* Genome analyses of single human oocytes. *Cell* **155,** 1492–1506 (2013).
33. Kleckner, N. Chiasma formation: chromatin/axis interplay and the role(s) of the synaptonemal complex. *Chromosoma* **115,** 175–194 (2006).
34. Novak, I. *et al.* Cohesin Smc1beta determines meiotic chromatin axis loop organization. *J. Cell Biol.* **180,** 83–90 (2008).
35. Klein, F. *et al.* Localization of RAP1 and topoisomerase II in nuclei and meiotic chromosomes of yeast. *J. Cell Biol.* **117,** 935–948 (1992).
36. Moens, P. B. & Earnshaw, W. C. Anti-topoisomerase II recognizes meiotic chromosome cores. *Chromosoma* **98,** 317–322 (1989).
37. Kleckner, N., Zickler, D. & Witz, G. Chromosome capture brings it all together. *Science* **342,** 940–941 (2013).
38. Agostinho, M. *et al.* Conjugation of human topoisomerase 2α with small ubiquitin-like modifiers 2/3 in response to topoisomerase inhibitors: cell cycle stage and chromosome domain specificity. *Cancer Res.* **68,** 2409–2418 (2008).
39. Lee, M. T. & Bachant, J. SUMO modification of DNA topoisomerase II: trying to get a CENse of it all. *DNA Repair* **8,** 557–568 (2009).
40. Kawamura, R. *et al.* Mitotic chromosomes are constrained by topoisomerase II-sensitive DNA entanglements. *J. Cell Biol.* **188,** 653–663 (2010).
41. Pope, L. H., Xiong, C. & Marko, J. F. Proteolysis of mitotic chromosomes induces gradual and anisotropic decondensation correlated with a reduction of elastic modulus and structural sensitivity to rarely cutting restriction enzymes. *Mol. Biol. Cell* **17,** 104–113 (2006).
42. Libuda, D. E., Uzawa, S., Meyer, B. J. & Villeneuve, A. M. Meiotic chromosome structures constrain and respond to designation of crossover sites. *Nature* **502,** 703–706 (2013).
43. Warsi, T. H. in *Centromeric Functions and Dynamics of DNA Topoisomerase II in S. cerevisiae* 130–187. Ph.D. thesis, Univ. California Riverside (2009).

Supplementary Information is available in the online version of the paper.

Acknowledgements We thank M. Hochstrasser, J. Bachant, S. Jentsch, L. Pillus and M. Weinreich for plasmids, J. Fung for Zip2 focus data, D. Zickler for the image in Fig. 6a, and members of the Kleckner laboratory and D. Zickler for advice and discussions. This research, L.Z., S.W., S.Y. and N.K. were supported by a grant to N.K. from the National Institutes of Health (RO1 GM044794); S.H. and K.P.K. were supported by the National Research Foundation of Korea funded by the Ministry of Science, ICT and Future Planning (2012-M3A9C6050367).

Author Contributions L.Z. and N.K. conceived and designed experiments, analysed data and wrote the paper. L.Z., S.W., Y.S., S.H. and K.P.K. performed experiments.

Author Information Reprints and permissions information is available at www.nature.com/reprints. The authors declare no competing financial interests. Readers are welcome to comment on the online version of the paper. Correspondence and requests for materials should be addressed to N.K. (kleckner@fas.harvard.edu).

METHODS

Strains. Yeasts strains are isogenic derivatives of SK1 (Extended Data Table 1) except for BR strains (Fig. 5), for which Zip2 foci data were provided by J. Fung (ref. 18).

Pachytene Zip2/Zip3 foci mark the sites of patterned ('interfering') crossovers. In budding yeast, as in many organisms, the majority of crossovers arise as the consequence of the programmed patterning process characterized by crossover interference. However, a minority of crossovers arise in some other way. The two types of crossover are referred to as 'patterned', 'class I' or 'interfering', and as 'class II' or 'non-interfering', respectively. We prefer to avoid the terms 'interfering' and 'non-interfering' for reasons discussed below.

There are a total of approximately 90 crossovers per yeast nucleus per round of meiosis as defined both by microarray and genetic analyses[44–46]. Mutant analysis suggests that the patterned (class I) crossovers constitute about 70% of total crossovers (estimates range from 60% to 90% in different studies; see, for example, refs 47, 48). Approximately 70% of about 90 total crossovers implies about 63 patterned (class I) crossovers per nucleus.

Zip2/3 foci appear to specifically mark the sites of patterned (class I) crossovers by several criteria, as follows.

First, there are approximately 65 foci of Zip2, Zip3 and Msh4/5 on yeast pachytene chromosomes per nucleus, and these different types of focus are highly co-localized with one another, implying that they mark the same specific set of recombinational interactions[8,19,49–51]. These foci also co-localize with DSBs formation/repair components, for example Mre11 and Rad51/Dmc1, implying that they mark the sites of recombinational interactions (see, for example, refs 18, 19, 50; L.Z., unpublished observations). The number of these foci corresponds well with the predicted number of patterned crossovers (above). Furthermore, crossover levels defined genetically co-vary with the number of Zip2/3 and Msh4/5 foci in mutants examined, for example *sgs1Δ*, *tel1Δ* and *spo11* hypomorphs, implying that they represent an important majority of recombinational interactions (refs 24, 52, 53 and this study). Additionally, Zip2/3 and Msh4/5 have all been implicated specifically in maturation of patterned/interfering crossovers (see, for example, refs 8, 18, 19, 44, 50, 51).

Second, Zip2 and Zip3 foci exhibit robust interference as shown both by coefficient of coincidence relationships for random adjacent pairs of intervals and by full coefficient of coincidence relationships along specific individual chromosomes (refs 8, 18 and this study). Also, the number of Zip3 foci shows crossover homeostasis as defined in strains with altered DSB levels (refs 8, 53 and this study), where homeostasis is dependent upon the presence of crossover interference (refs 8, 24 and this study). In contrast to Zip2/3 foci, total crossovers show much weaker interference[8].

Third, our beam-film model can accurately explain total crossover patterns (including coefficient of coincidence relationships and the event distribution for total crossovers) by assuming that Zip2/3 foci mark the sites of patterned (class I) crossovers; that class II crossovers represent ~30% of total crossovers; and, furthermore, that class II crossovers arise from the interactions that are 'leftover' after the operation of crossover designation and interference[8]. These 'leftover' interactions are usually matured without exchange of flanking markers; that is, to 'non-crossover' products. However, as proposed in ref. 15 and modelled in our analysis, these interactions may sometimes proceed to a crossover outcome instead of a non-crossover outcome, thus giving class II crossovers. Such a mixture of non-crossovers and a few crossovers would make the outcome for leftover meiotic interactions similar to the outcome of mitotic DSB repair.

We also note that the term 'non-interfering' is misleading when applied to class II recombinational interactions. In budding yeast, as in several (possibly all) other organisms, total recombinational interactions tend to be evenly spaced along each bivalent[8]. As a result, not only will patterned/class I crossovers exhibit interference, so too will total interactions and class II crossovers; moreover, class II crossovers will interfere with patterned (class I) crossovers[8].

Fourth, both Zip2 and Zip3 foci occur specifically on the association sites between homologues in *zip1Δ* chromosomes[18,50]. Analysis of Zip2 foci reveals that they exhibit interference[8,18]. Moreover, they exhibit the same level of interference along *zip1Δ* chromosomes as along WT chromosomes when the metric of interference is physical distance (Fig. 5).

We note that this robust cytological interference contrasts with the fact that, by genetic analysis, crossover interference is significantly compromised in a *zip1Δ* mutant (see, for example, refs 44, 54). It also can be noted that cytological and genetic studies were performed in different strain backgrounds (BR at 30 °C and SK1 at 30 °C, respectively). This is because (1) in BR at 30 °C, *zip1Δ* chromosomes are well formed to permit cytological analysis but meiosis arrests during prophase, thus precluding genetic analysis of recombination outcomes, whereas (2) in SK1 at 30 °C, *zip1Δ* chromosomes are less well formed, thus making cytological analysis more difficult, whereas meiosis does not arrest, thus permitting genetic analysis.

One possible explanation for the absence of genetic interference in the *zip1Δ* mutant can be excluded. In principle, crossover designation and interference might occur normally and then be followed by a crossover-specific 'maturation defect'; that is, a defect in the probability that designated interactions will actually mature to detectable crossovers. This progression is not acceptable because, in such a situation, the detectable crossovers that do manage to form will still exhibit normal interference[8]. By contrast, a diagnostic maturation effect can be seen in an *mlh1Δ* mutant[8,55].

Two other, not mutually exclusive, explanations for absence of genetic interference in *zip1Δ* can be suggested, as follows.

- In WT meiosis, crossover interference is fundamentally a structure-based process to which DNA events are biochemically coupled as a downstream consequence. By this view, Zip1 would not be required for local 'crossover designation' and interference at the structural level but would be required either (1) to set up coupling between crossover/non-crossover decisions and biochemical events and/or (2) to transduce the structural interference signal into the appropriate biochemical outcome. It appears that crossover designation is a specifically programmed outcome and interactions that are not crossover-designated mature instead to non-crossovers as the default option[15,24]. It further appears that some of these 'non-crossover-fated' interactions may actually mature into crossover products, thus giving the 'non-patterned' crossovers that are not marked by Zip3 foci[8]. Thus, in possibility (1), all interactions might progress to the 'non-crossover' outcome, giving an increase in non-crossovers and some crossovers as well, with those crossovers exhibiting the same distribution as total precursor interactions. This is, in fact, the phenotype observed at the *HIS4LEU2* hot spot in SK1 *zip1Δ* at 30 °C[14]. In possibility (2), crossover/non-crossover differentiation would occur at the biochemical level but there would be no progression of crossover-fated interactions. This is, in fact, the phenotype observed at the *HIS4LEU2* hot spot in SK1 *zip1Δ* at 33 °C (ref. 14).
- A reduction in the frequency of mature patterned (class I) crossovers might be accompanied by an increase in the frequency of crossovers from other sources, for example occurrence of additional DSBs, some of which then give rise to crossovers[56]. Attempts to model this situation with beam-film simulations suggest that the level of extra events required to confer the strong defect in crossover interference observed in *zip1Δ* is very high (L.Z., unpublished observations). Thus, this effect may contribute to, but not be the sole basis for, absence of crossover interference in *zip1Δ*.

Fifth, localization of Zip3 along yeast chromosomes has been evaluated molecularly by chromatin immunoprecipitation (ChIP) analysis[57]. This analysis identifies peaks and valleys of Zip3 abundance, genome wide, at different times of meiosis, and relates the positions of those peaks to peaks of Rec8 and Red1 (markers for chromosome axes at mid-prophase) and to peaks corresponding to DSB sites (marked by single-stranded (ss)DNA in a *dmc1Δ* strain). Zip3 is initially most prominent at centromere regions. This localization, which corresponds to the early leptotene Zip1 centromere association seen cytologically, is independent of DSB formation; it is prominent at $t = 3$ h, about the time of DSB formation; and it mostly disappears by $t = 5$ h, the time of pachytene when Zip3 foci are assayed here. Correspondingly, we find no tendency for Zip3 foci to occur at centromeres in pachytene (L.Z., unpublished observations). At $t = 4$ and 5 h, Zip3 appears in co-localization with chromosome axis markers and DNA DSB sites. Axis-localization slightly precedes DSB site localization and remains high while DSB site localization increases prominently, apparently in correlation with post-crossover-designation crossover-specific events. It is very difficult to make any relationship between ChIP results and cytological focus analysis for several reasons. (1) ChIP analysis looks at a population average localization, not a per-nucleus localization. (2) At $t = 4$ h, most cells are in leptotene/zygotene, which we do not examine cytologically. Moreover, even at $t = 5$ h, only ~50% of cells are in pachytene. Thus, ChIP data include significant signals from irrelevant stages. (3) The resolution of ChIP analysis is ~1–5 kb, with axis-association sites tending to alternate with DSB sites at separations of 5–10 kb (refs 11, 57). In contrast, Zip3 foci extend ~300 nm along the chromosome (0.3 ± 0.06 μm; $n = 320$), which corresponds to ~90 kb in the present study (average for chromosomes III, IV and XV). Thus, a single Zip3 focus can encompass multiple axis association and DNA DSB sites. Correspondingly, ChIP analysis may well be detecting sub-focus level alterations within a crossover-designated region that reflect changes in the intimate molecular crosslinkability of Zip3 molecules to different types of DNA segment without any change in the position of the associated Zip3 focus. For example, the finding of more prominent ChIP localization to DSB sites in mutants that progress farther into recombination may reflect the extent to which those sequences are no longer buried within earlier recombination complexes. (4) To complicate matters further, it is clear cytologically that a low level of Zip3 localizes all along pachytene chromosome axes beyond that present in prominent foci. This general background will be detected in ChIP analysis but not by Zip3 focus analysis.

Visualization and definition of synaptonemal complex lengths and Zip3 focus positions (additional details in ref. 8). Meiotic time courses and sample preparation. Appropriately pre-grown cell cultures were taken through synchronous meiosis by the SPS method[58,59], with meiosis initiated by transfer of cells to sporulation medium ($t = 0$). Cells were harvested at $t \approx 4$–5 h, the time at which pachytene cells are most abundant (constituting approximately 50% of all cells). Harvested cells were spheroplasted to remove the cell wall and then re-suspended in MES wash (1 M sorbitol, 0.1 M MES, 1 mM EDTA, 0.5 mM $MgCl_2$ pH 6.5). Cells were then lysed and spread on a glass microscope slide with 1% Lipsol (LIP) and fixed by 3% w/v paraformaldehyde with 3.4% w/v sucrose as described in ref. 60.

Fluorescence visualization. Glass slides with spread nuclei were incubated at room temperature for 15 min in 1× Tris buffered saline (TBS) buffer (25 mM Tris-Cl, pH 8, 136 mM NaCl, 3 mM KCl) then blocked with 1× TBS buffer with 1% w/v bovine serum albumin (BSA) for 10 min. Chromosomes in spread nuclei were then stained with appropriate antibodies. Primary antibodies were mouse monoclonal anti-myc (for detection of Zip3-Myc), goat polyclonal anti-Zip1 (Santa Cruz) and rabbit polyclonal anti-GFP, diluted 1:1,000 in 1× TBS with 1% BSA. Secondary antibodies were anti-mouse, anti-goat and anti-rabbit IgG labelled with Alexa Fluor 488, 594 or 555 (Molecular Probes), respectively; all were diluted 1:1,000 in 1× TBS with 1% BSA. Slides were mounted in Prolong Gold antifade (Molecular Probes). For condensin mutants and *spo11* hypomorphs with very low DSB levels, Zip1 staining was less bright than in WT, so axes were usually visualized by immunostaining of Rec8-3HA with rat anti-HA primary antibody and anti-rat labelled with Alexa Fluor 647 or 594 secondary antibody. Control experiments confirmed that the same synaptonemal complex lengths and Zip3 focus numbers/distributions/coefficient of coincidence relationships were obtained with either Zip1 or Rec8 staining. Stained chromosome spreads were visualized on an Axioplan IEmot microscope (Zeiss) using appropriate filters. Images were collected using Metamorph (Molecular Devices) image acquisition.

Defining Zip3 focus positions and synaptonemal complex lengths. Images for Zip3, Zip1 (or Rec8) and *LacO*/LacI–GFP staining (text Fig. 1a, b) were merged and aligned. The GFP-marked chromosome was analysed in nuclei where it was unambiguously separated from other chromosomes. The segmented line-tracing tool of Image J software (National Institutes of Health) was used. Each trace was initiated at the centre of the GFP focus, which typically falls beyond the end of the synaptonemal complex (white line in Fig. 1b). The trace was continued following the path of the Zip1 (Rec8) signal for the entire length of the chromosome. As the trace encountered a position judged (by eye) to be the centre of a Zip3 focus, that position was annotated using the 'mark position' function (control M). By application of the 'zoom' function, the annotated position of each Zip3 focus could be defined at the one-pixel level (~0.067 μm under our microscope). The distal end of the Zip1 (Rec8) signal was also annotated. Synaptonemal complex length was given by the annotated position mark at the end of the trace. Importantly, by this approach, each Zip3 focus (and the value for total synaptonemal complex length) was subject to its own positioning error (evaluated below) with no accumulation of error along the trace.

Accuracy of Zip3 focus (synaptonemal complex length) positions. The accuracy of the results obtained by the above approach was evaluated in several ways. (1) Coefficient of coincidence curves are highly reproducible in multiple experiments of the same strain, as shown by the correspondence of coefficient of coincidence values among different chromosomes (Fig. 1d) and for four independent analyses of a single chromosome[8]. (2) The intensity of Zip3 can be determined quantitatively along the trace and the positions of intensity peaks compared with the positions of foci defined by eye. The two methods give virtually identical results except that the eye can distinguish a significant number (~5%) of foci that are not, or less, obvious in the trace (for example, as shoulders on major peaks). (3) To determine the precision with which each focus position (or each synaptonemal complex length) is defined in a given trace, chromosome XV was traced six times in each of four nuclei. The four bivalents exhibited four Zip3 foci (one case) or five Zip3 foci (three cases). The variation in the absolute position of a given focus (or synaptonemal complex length) among a set of six duplicate traces ranged from 0 to 0.14 μm with an average of 0.08 μm (80 nm). Furthermore, for each focus among six traces, the standard deviation of this variation ranged from 0.02 to 0.04 μm. In summary, the absolute position of each Zip3 focus (or total synaptonemal complex length) for a given traced bivalent is specified with an accuracy of approximately one pixel (67 nm).

We also performed reconstruction experiments to assess the possible effects of one-pixel accuracy on coefficient of coincidence curves. For four WT and two *pCLB2-TOP2* experimental data sets, independently, Zip3 focus positions were subjected to computational 'adjustment', with the position of each focus moved by one pixel in one direction or the other, randomly for different foci. The coefficient of coincidence curve was then re-calculated. The values of L_{CoC} were not changed (0.3 ± 0.01 μm before and after 'adjustment'; further discussion of the accuracy of the coefficient of coincidence curves below). There were very subtle changes in the shape of the coefficient of coincidence curve. However, the nature of these changes in fact suggests that the relationships from the position-randomized data set represent a degradation of the more robust interference relationships observed in the primary data. (1) At smaller inter-interval distances (<0.2 μm), coefficient of coincidence values are slightly higher. This is expected by the fact that randomized movement will artificially increase the fraction of closer-together focus pairs. (2) At larger inter-interval distances, coefficient of coincidence values fail to rise above one. This is expected because randomized movement will reduce the tendency for the inter-focus position to exhibit a node at the most likely inter-crossover position(s) (further explanation in next section).

Analysis of Zip3 focus (crossover) patterns: coefficient of coincidence and modified coefficient of coincidence relationships. *Coefficient of coincidence relationships (see, for example, Fig. 1d).* The coefficient of coincidence analysis is the classic indicator of crossover interference[61]. If done correctly (with a sufficiently large number of intervals) with a sufficiently large data set, coefficient of coincidence curves provide a highly accurate description of crossover patterns (discussion in ref. 8). We note that, in contrast, mathematical analysis of 'evenness' by application of the gamma distribution, while 'model-independent', can give a misleading impression with respect to mutant phenotypes or other types of variation (discussion in ref. 8). For example, a defect in maturation of crossovers after their positions have been designated has no effect on interference and thus does not affect coefficient of coincidence relationships but significantly alters the value of the gamma 'evenness' parameter. Coefficient of coincidence curves for Zip3 foci were obtained using the 'Analyze crossover data' feature of the beam-film program, using as an input the experimentally defined positions of Zip3 foci in a given experiment[8]. For this purpose, chromosomes are divided into a number of intervals with equal size (detailed discussions in ref. 8 protocol S1). For each interval the total frequency of Zip3 foci in the set of chromosomes examined is determined. Then, for each pair of intervals, the observed frequency of chromosomes exhibiting a Zip3 focus in both intervals (referred to for convenience as 'double crossovers') is determined. This value defines the frequency of 'observed double crossovers'. If crossovers (Zip3 foci) arise independently in each interval, the predicted frequency of double crossovers for a given pair of intervals should be the product of the frequencies of crossovers (Zip3 foci) in the two intervals considered individually. This product is the frequency of 'expected double crossovers'. The coefficient of coincidence for that particular pair of intervals is the ratio of these two frequencies, that is the observed/expected ratio for that interval pair. A coefficient of coincidence curve is obtained by considering all possible pairs of intervals, with the coefficient of coincidence value for each pair plotted as a function of the distance between (the midpoints of) the two corresponding intervals. For a classic coefficient of coincidence curve, at very small inter-interval distance, the coefficient of coincidence is close to zero, indicating very strong crossover interference. As the inter-interval distance increases, the coefficient of coincidence also gradually increases, indicating that crossover interference decreases with increased inter-interval distance. Eventually, the coefficient of coincidence value reaches one, implying that, at the corresponding inter-interval distance, crossover interference no longer has any influence. At certain specific larger inter-interval distances, the coefficient of coincidence value tends to be greater than one, implying that, at these distances, there is a higher probability of double crossovers than predicted on the basis of independent occurrence. Nodes of coefficient of coincidence greater than 1 tend to occur at inter-interval distances that correspond approximately to the average inter-crossover distance and multiples thereof (see ref. 8 for more examples). This pattern reflects the fact that operation of crossover interference tends to create an evenly spaced array of crossovers (Zip3 foci, in this analysis).

For convenience, the inter-interval distance at which the coefficient of coincidence = 0.5 is defined as L_{CoC} and can be used as a measurement for 'crossover interference strength', by which is meant the effective distance over which crossover interference acts. Importantly, at a mechanistic level, variations in L_{CoC} can result from variations in features other than the distance over which the interference signal spreads (for example, as discussed for beam-film simulations below). Values of L_{CoC} are highly reproducible from one experiment to another. For the three analysed chromosomes in WT meiosis, values for individual experiments and the averages and standard deviations are as follows: chromosome XV, 0.31, 0.3, 0.32, 0.32 (0.31 ± 0.01; $n = 4$); chromosome III, 0.31, 0.32, 0.3 (0.31 ± 0.01; $n = 3$); chromosome IV, 0.31, 0.32 (0.32 ± 0.01; $n = 2$). Further documentation is in ref. 8.

Modified coefficient of coincidence analysis (Fig. 1e). As an alternative approach to evaluating the effective interference distance, we adapted the 'modified coefficient of coincidence' approach previously described for analysis of genetic crossover data[21]. For the present purpose, each interval is used as a reference (Ref; Fig. 1e top left). Chromosomes are then divided into two groups: those with or without a crossover (Zip3 focus) in this reference interval (CO^+_R or CO^-_R). Another nearby

interval is then selected as a test (Test (T)). For each reference group (CO^+_R or CO^-_R), the numbers of chromosomes with and without a crossover in this test interval is determined (CO^+_T and CO^-_T). If crossover levels are lower in the CO^+_R group than in the CO^-_R group, the presence of a crossover in the reference interval has reduced the probability of a crossover in the Test interval; that is, interference emanating from the reference interval has been felt in that Test interval. When this evaluation is performed for all intervals in the vicinity of a given reference interval, it reveals the distance over which interference extends outward from that interval, giving L_{MCoC} for that reference interval (Fig. 1e, top right). Determination of L_{MCoC} values for all intervals along each of the three analysed chromosomes gives an average L_{MCoC} for that chromosome (Fig. 1e, bottom right).

This analysis requires an evaluation, for each comparison between a reference interval and a test interval, of whether the relative frequencies of CO^+_T and CO^-_T chromosomes are the same for the CO^+_R and CO^-_R groups or different (that is, lower in the CO^+_R group). For this purpose, Fisher's exact test was applied. Since interference is stronger (and thus more likely to be statistically significant) at shorter distances, the more stringent the probability specified by Fisher's exact test, the shorter the inferred 'interference distance'. The standard criterion for significance by this method is $P < 0.05$. By this criterion, L_{MCoC} for the three analysed chromosomes in WT meiosis was 0.3 μm, which is the same as L_{CoC} as defined above. With a more stringent criterion, $P < 0.01$, L_{MCoC} is slightly shorter (0.25 μm). Importantly, mutants with decreased interference distance always showed decreased L_{MCoC} compared with WT regardless of whether the standard, or more stringent, criterion was applied. Thus, when $P < 0.05$, L_{MCoC} in *top2* mutants versus WT was 1.3 intervals versus 1.9 intervals (that is, 0.2 μm versus 0.3 μm); when $P < 0.01$, L_{MCoC} in *top2* mutants versus WT was 1.0 versus 1.5 in WT (that is, 0.16 μm versus 0.25 μm). Given that $P < 0.05$ is the standard value applied for Fisher's exact test and the fact that L_{CoC} and L_{MCoC} correspond at $P < 0.05$, we adopted this level of stringency to describe L_{MCoC} in the present analysis (Figs 1, 2 and 4 and Extended Data Fig. 3).

Beam-film simulations. The beam-film model and the program used for simulations are described in detail in refs. 4 and 8. The beam-film program was recently rewritten in MATLAB (R2010a), which is downloadable at https://app.box.com/s/hv91q2nrtq0cp9n8iy9m.

Outline of the beam-film model. An array of precursor interactions comes under global stress, which causes a first (most sensitive) precursor to go critical, undergoing a stress-promoted change that commits it to becoming a crossover ('crossover designation'). The intrinsic effect of this change will be a local reduction in the level of stress at the site of the change. To even out distribution of stress along the chromosome, the initial local reduction in stress then redistributes outwards in both directions, thus reducing the probability that any subsequent crossover designation(s) will occur in the affected region. This effect constitutes crossover interference. Assuming that the system does not comprise a single elastic component, the extent of stress reduction will dissipate with increasing distance away from the nucleation site, becoming negligible over a characteristic distance (corresponding to the 'interference distance'). A second crossover designation may then occur. If so, that crossover will occur preferentially at a position that retains a high stress level and thus preferentially at some distance away from the position of the prior crossover designation. This second crossover designation will again result in local stress relief and redistribution (and thus interference), giving a new stress landscape along the chromosome. If/as additional events occur, they will tend to fill in the holes between prior events, thus giving an evenly spaced array. The beam-film model predicts the number and array of crossovers that will occur in particular system with particular mechanical properties that are analogous to a known system in the physical world (the 'beam-film system'). In this particular system, the magnitude of the stress reduction decreases exponentially with distance away from its nucleation point.

Beam-film best-fit simulations. In beam-film simulation analysis, the parameters of the beam-film model are varied to define the constellation of parameter values at which the predicted array of crossover events best matches that observed experimentally for a particular data set[8]. As described in detail elsewhere[8], the parameters to be specified fall into three categories that describe, respectively, the following: (1) the array of precursor interactions upon which crossover patterning acts; (2) the nature of the patterning process per se; and (3) the probability that a crossover-designated interaction will actually mature to an experimentally detectable crossover or crossover marker (that is, a Zip3 focus).

For modelling, the level of global stress is progressively increased up to a maximum specified level (S_{max}). As the level of stress increases, precursors will undergo crossover designation sequentially in relation to their relative local stress levels at that moment in the sequence of events (differently for different bivalents according to their specific histories). Each crossover designation triggers reduction in stress, in both directions, over a characteristic length given by a specific parameter (L). The value of L for a particular simulation is directly reflected in the resultant coefficient of coincidence relationships and corresponds very closely to the inter-interval distance at which the coefficient of coincidence = 0.5, defined here as L_{BF}. A third patterning parameter ('A') describes precursor reactivity: that is, the way in which the probability of crossover designation varies as a function of the local stress level at the corresponding position. A fourth patterning parameter ('clamping') permits adjustment of crossover probabilities near chromosome ends.

Parameter values for beam-film best-fit simulations of crossovers (Zip3 foci) along WT yeast chromosomes are described in ref. 8. The best-fit simulations for mutant patterns presented in Figs 2a, 3a–c and 4a, b (except mutants with altered axis lengths) were obtained using these same parameter values except that the value of L was appropriately reduced, from ~0.3 μm to ~0.2 μm, resulting in a commensurate reduction in L_{BF}. Best-fit simulations in situations with altered DSB levels (Fig. 2d) also involved changes in the number of precursors (N), as discussed below ('crossover homeostasis analysis') and in Extended Data Fig. 4. Best-fit simulations in mutants with altered axis lengths also involved changes in the number of precursors (N), as discussed in Extended Data Fig. 9.

Crossover homeostasis analysis. Crossover homeostasis is a nonlinear relationship between the number of DSBs and the number of crossovers[8,24]. The existence and magnitude of crossover homeostasis depends on the existence and strength of crossover interference (see text and ref. 8).

Beam-film simulations of crossover homeostasis. A beam-film best-fit simulation predicts the number of crossovers that will occur if crossover designation and interference occur according to a specific set of values for involved parameters. To get a simulated crossover homeostasis curve under a particular set of conditions, multiple beam-film simulations were performed at different values of the precursor number N, which were varied over a desired range, and with the values of all other parameters held constant. The average numbers of crossovers predicted for each evaluated value of N were then plotted as a function of N. Such curves were then obtained analogously at different values for the interference distance L (ref. 8; Fig. 2d).

Experimental evaluation of crossover homeostasis by Zip3 focus analysis. The positions of Zip3 foci were determined along specific marked chromosomes (XV and III) in a series of strain backgrounds known to give varying levels of DSBs, in both a *TOP2* and a *pCLB2-TOP2* background. Coefficient of coincidence relationships and the numbers and distributions of Zip3 foci per bivalent for all strains are given in Figs 1 and 2 and Extended Data Figs 2 and 4. Average Zip3 focus numbers per chromosome (average ± s.d.) are shown in Fig. 2d and listed in the legend to Extended Data Fig. 4.

DSB levels were decreased below WT levels by a previously described series of hypomorphic *spo11* alleles (*spo11HA*, *spo11YFHA*, spo11*DAHA*; ref. 24). DSB levels were increased above WT levels using a *tel1Δ* mutation, alone and in combination with a *spo11* hypomorph (*tel1Δ spo11 HA*). The average numbers of Zip3 foci per bivalent in the different strains were then plotted as a function of beam-film precursor or DSB level (discussion below). Such analysis was in strain backgrounds that were also either (1) WT for crossover interference (*TOP2*) or (2) carried the *pCLB2-TOP2* construct that resulted in meiotic depletion of topoisomerase II (see text).

The number of DSBs per bivalent in a *TOP2* strain with WT DSB formation can be accurately determined on the basis of comprehensive evaluation results from DSB mapping (for example, ref. 12), microarray (for example, ref. 45) and classic genetic measurements (http://www.yeastgenome.org). The numbers of DSBs on chromosomes III, IV and XV are thus defined as 6, 19 and 13 respectively. The relative levels of DSBs in strains carrying *spo11* mutations has been evaluated in a *TOP2* background by gel electrophoresis in a *rad50S* background[24] (where DSBs do not turn over). In the *tel1Δ* mutant, DSBs are increased by ~50% at the *HIS4LEU2* locus in a *rad50S* background without significantly altering crossover interference[8,62] (Extended Data Fig. 7 and L.Z., unpublished observations).

However, in some regions and circumstances, *rad50S* DSB levels are known to be lower than the level of DSBs in *RAD50* meiosis (see, for example, refs 11, 12). Furthermore, *rad50S* analysis of *spo11/tel1Δ* alleles in a *pCLB2-TOP2* background has not been performed. We therefore also evaluated DSB levels by application of beam-film analysis. For all strains analysed for Zip3 focus patterns, both *TOP2* and *pCLB2-TOP2*, best-fit beam-film simulations were defined[8] (Figs 2–4 and Extended Data Figs 2 and 4). For each strain, all parameter values were held constant at those defined for the two *SPO11 TEL1* cases (see text) except that the average number of precursors per bivalent (N) was varied to determine the value that gave the optimal match between observed and predicted crossover patterns for that strain. Beam-film-predicted DSB/precursor levels were the same for the *TOP2* and *pCLB2-TOP2* versions of all strains (Figs 2–4 and Extended Data Fig. 4c). This prediction matches the experimental finding that *TOP2* and *pCLB2-TOP2* strains exhibit the same level of total inter-homologue events (crossover plus non-crossover) at *HIS4LEU2* in a *RAD50 SPO11 TEL1* background (Extended Data Fig. 8). Furthermore, for *TOP2* strains, DSB/precursor

values obtained by beam-film simulations are very similar to those obtained on the basis of *rad50S* analysis (Extended Data Fig. 4c). Correspondingly, crossover homeostasis relationships are very similar regardless of whether DSBs or beam-film-predicted precursors are used as the metric (Fig. 2d and Extended Data Fig. 4d).

Interestingly, experimentally determined *rad50S* DSB levels tend to be slightly lower than those predicted by beam-film analysis, especially at lower DSB levels (Extended Data Fig. 4). Moreover, experimental data match beam-film-predicted crossover homeostasis relationships somewhat more accurately when the metric of the DSB level is the beam-film-predicted precursor level, especially at lower DSB/precursor levels (Extended Data Fig. 4d). This correspondence suggests that beam-film-predicted values may be more accurate than *rad50S* experimental values. Data in ref. 24 support this conclusion: at *HIS4LEU2*, a *spo11HA/HA* strain exhibits 50% of the *SPO11* level of *rad50S* DSBs but 62% of the level of inter-homologue recombination products (crossover plus non-crossover), implying a deficit of 20% by *rad50S* analysis. Similarly, a *spo11HA/DA* strain exhibits 20% of the *SPO11* level of *rad50S* DSBs but 27% the level of inter-homologue recombination products, a deficit of 26%.

These analyses also provide further evidence (in addition to that presented in Extended Data Fig. 7) that the increased number of Zip3 foci seen in *top2* mutants compared with *TOP2* strains cannot be explained as increased DSBs.

44. Chen, S. Y. *et al.* Global analysis of the meiotic crossover landscape. *Dev. Cell* **15,** 401–415 (2008).
45. Mancera, E., Bourgon, R., Brozzi, A., Huber, W. & Steinmetz, L. M. High-resolution mapping of meiotic crossovers and non-crossovers in yeast. *Cell* **454,** 479–485 (2008).
46. Cherry, J. M. *et al.* Genetic and physical maps of *Saccharomyces cerevisiae*. *Nature* **387,** 67–73 (1997).
47. Argueso, J. L., Wanat, J., Gemici, Z. & Alani, E. Competing crossover pathways act during meiosis in *Saccharomyces cerevisiae*. *Genetics* **168,** 1805–1816 (2004).
48. de los Santos, T. *et al.* The Mus81/Mms4 endonuclease acts independently of double-Holliday junction resolution to promote a distinct subset of crossovers during meiosis in budding yeast. *Genetics* **164,** 81–94 (2003).
49. Hollingsworth, N. M., Ponte, L. & Halsey, C. MSH5, a novel MutS homolog, facilitates meiotic reciprocal recombination between homologs in *Saccharomyces cerevisiae* but not mismatch repair. *Genes Dev.* **9,** 1728–1739 (1995).
50. Chua, P. R. & Roeder, G. S. Zip2, a meiosis-specific protein required for the initiation of chromosome synapsis. *Cell* **93,** 349–359 (1998).
51. Shinohara, M., Oh, S. D., Hunter, N. & Shinohara, A. Crossover assurance and crossover interference are distinctly regulated by the ZMM proteins during yeast meiosis. *Nature Genet.* **40,** 299–309 (2008).
52. Jessop, L., Rockmill, B., Roeder, G. S. & Lichten, M. Meiotic chromosome synapsis-promoting proteins antagonize the anti-crossover activity of Sgs1. *PLoS Genet.* **2,** e155 (2006).
53. Henderson, K. A. & Keeney, S. Tying synaptonemal complex initiation to the formation and programmed repair of DNA double-strand breaks. *Proc. Natl Acad. Sci. USA* **101,** 4519–4524 (2004).
54. Sym, M. & Roeder, G. S. Crossover interference is abolished in the absence of a synaptonemal complex protein. *Cell* **79,** 283–292 (1994).
55. Nishant, K. T. *et al.* The baker's yeast diploid genome is remarkably stable in vegetative growth and meiosis. *PLoS Genet.* **6,** e1001109 (2010).
56. Kauppi, L. *et al.* Numerical constraints and feedback control of double-strand breaks in mouse meiosis. *Genes Dev.* **27,** 873–886 (2013).
57. Serrentino, M. E., Chaplais, E., Sommermeyer, V. & Borde, V. Differential association of the conserved SUMO ligase Zip3 with meiotic double-strand break sites reveals regional variations in the outcome of meiotic recombination. *PLoS Genet.* **9,** e1003416 (2013).
58. Kim, K. P. *et al.* Sister cohesion and structural axis components mediate homolog bias of meiotic recombination. *Cell* **143,** 924–937 (2010).
59. Koszul, R. & Kleckner, N. Dynamic chromosome movements during meiosis: a way to eliminate unwanted connections? *Trends Cell Biol.* **19,** 716–724 (2009).
60. Loidl, J., Klein, F. & Engebrecht, J. Genetic and morphological approaches for the analysis of meiotic chromosomes in yeast. *Methods Cell Biol.* **53,** 257–285 (1998).
61. Charles, D. R. The spatial distribution of cross-overs in X-chromosome tetrads of *Drosophila melanogaster*. *J. Genet.* **36,** 103–126 (1938).
62. Zhang, L., Kim, K. P., Kleckner, N. E. & Storlazzi, A. Meiotic double-strand breaks occur once per pair of (sister) chromatids and, via Mec1/ATR and Tel1/ATM, once per quartet of chromatids. *Proc. Natl Acad. Sci. USA* **108,** 20036–20041 (2011).
63. Imai, S., Armstrong, C. M., Kaeberlein, M. & Guarente, L. Transcriptional silencing and longevity protein Sir2 is an NAD-dependent histone deacetylase. *Nature* **403,** 795–800 (2000).
64. Wu, C. S., Chen, Y. F. & Gartenberg, M. R. Targeted sister chromatid cohesion by Sir2. *PLoS Genet.* **7,** e1002000 (2011).
65. Dhillon, N. & Kamakaka, R. T. A histone variant, Htz1p, and a Sir1p-like protein, Esc2p, mediate silencing at HMR. *Mol. Cell* **6,** 769–780 (2000).
66. Derbyshire, M. K., Weinstock, K. G. & Strathern, J. N. HST1, a new member of the SIR2 family of genes. *Yeast* **12,** 631–640 (1996).
67. Hong, S. *et al.* The logic and mechanism of homologous recombination partner choice. *Mol. Cell* **51,** 440–453 (2013).

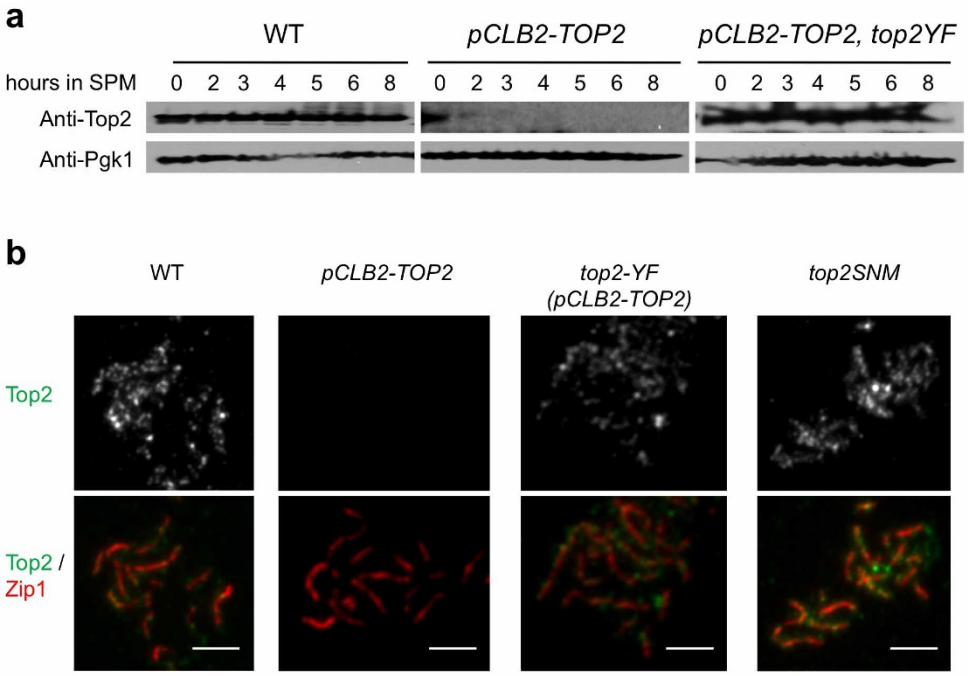

Extended Data Figure 1 | Top2 protein level and localization on chromosomes in three *top2* mutants. **a**, Top2 protein levels shown as a function of time after entry into meiosis ($t = 0$). Top2 levels are severely reduced in *pCLB2-TOP2* (middle panel) and are the same as WT in *pCLB2-TOP2 top2YF* (±20% relative to anti-Pgk1 control). Western blot analysis used anti-Top2 antibody (TopoGEN 2014) and anti-Pgk1 antibody (Abcam ab113687). **b**, Immunostaining of Top2 on meiotic chromosomes with the same antibody used for western blot analysis in **a**: at pachytene (shown) and at leptotene (data not shown). Top2 is undetectable on chromosomes in *pCLB2-TOP2* and is present at similar levels to WT in *pCLB2-TOP2 top2YF* and *top2SNM*. Chromosomes were concomitantly immunostained for Zip1 (Santa Cruz, sc-48716) as in text Fig. 1. Scale bars, 3 μm.

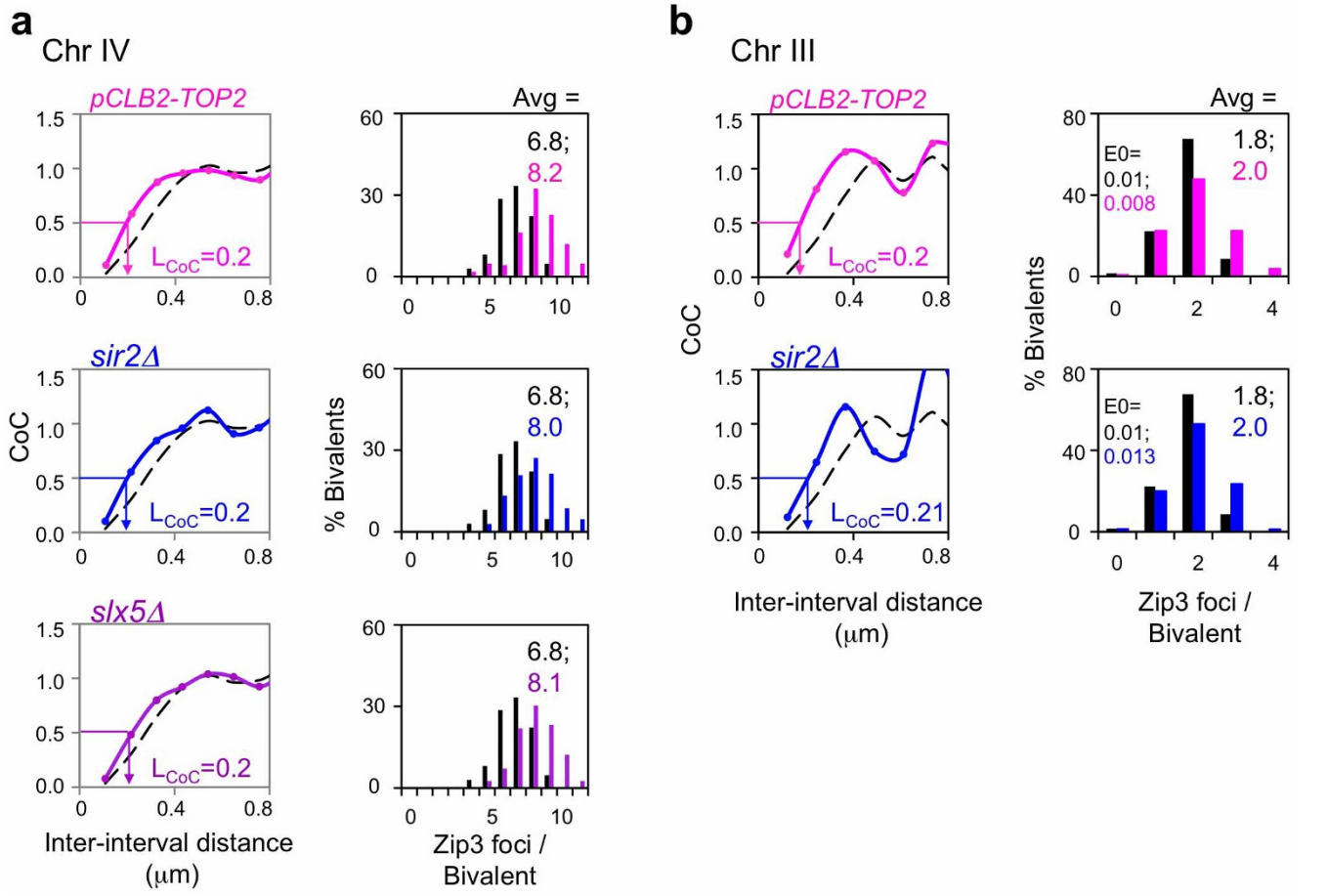

Extended Data Figure 2 | Decreased crossover interference in *pCLB2-TOP2* and *sir2Δ*, *slx5Δ* is confirmed on other chromosomes. a, b, The same decreases in crossover interference ($L_{CoC} \approx 0.2$ μm versus ≈ 0.3 μm in WT) and corresponding increases crossover number observed for the indicated mutants on chromosome XV (Figs 2 and 3) are also observed on chromosomes IV and III in *pCLB2-TOP2* and *sir2Δ*, and on chromosome IV in *slx5Δ*. Data for WT in black.

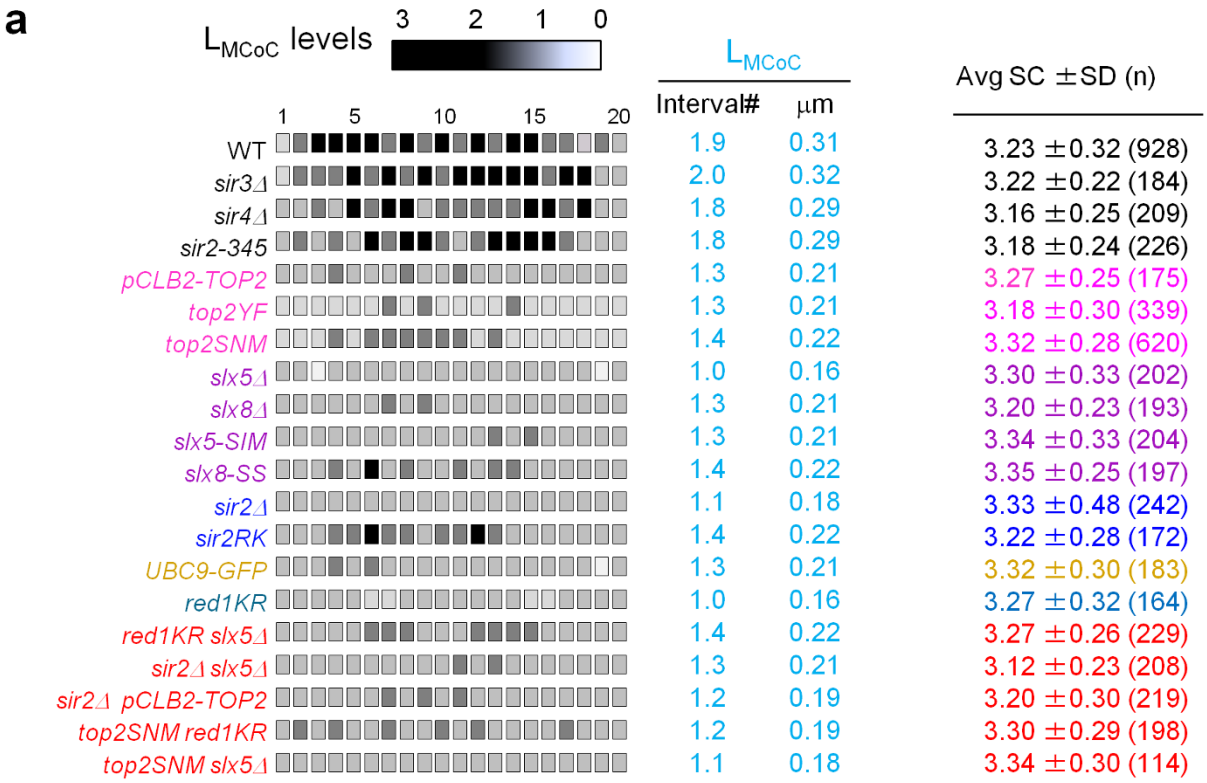

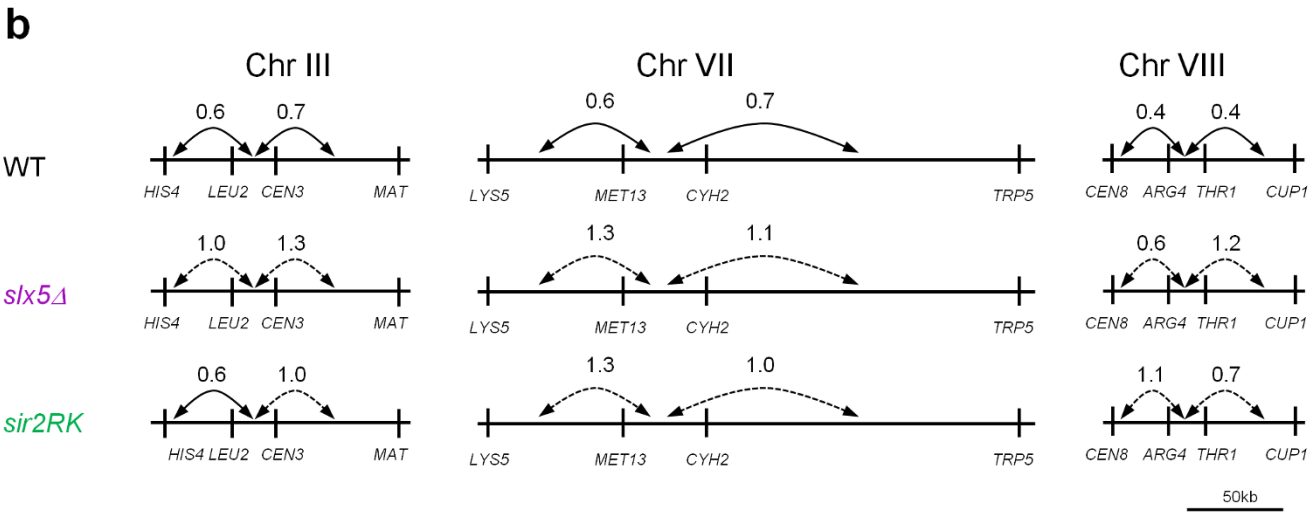

Extended Data Figure 3 | Decreased crossover interference as revealed by modified coefficient of coincidence and tetrad analysis using the method of ref. 21, but synaptonemal complex length is the same as in WT. a, By modified coefficient of coincidence analysis (Fig. 1; Methods), crossover interference can extend to about two intervals on either side of the reference interval ($L_{MCoC} \approx 0.3$ μm) in WT and in three *sir2* mutants that exhibit WT crossover patterning by other criteria ($L_{CoC} \approx 0.3$ μm; Fig. 3 and Extended Data Fig. 2). In contrast, in all examined single and double mutants where crossover interference is defective ($L_{CoC} \approx 0.2$ μm; Figs 2–4), crossover interference extends only about 1.3 intervals ($L_{MCoC} \approx 0.2$ μm) (for *top2* mutants, see also Fig. 2). Right column shows synaptonemal complex lengths for each of the analysed strains (average ± s.d.). There is no significant difference between strains exhibiting WT interference (average of averages is 3.25 ± 0.06 μm) and strains defective in the *top2* interference pathway (average of averages is 3.27 ± 0.07 μm). **b**, Decreased crossover interference in *slx5Δ* and *sir2RK* as revealed by tetrad analysis. Each pair of intervals was tested, reciprocally, for the ratio of the map distances in one interval with and without crossovers in the other interval. Each number shows the average of the ratios for the two reciprocal cases. A value less than 1 indicates crossover interference. Solid and dotted lines indicate whether the level of interference is statistically ($P < 0.05$ by *G*-test) significant or not, respectively. Genetic crossover interference is greatly decreased in *slx5Δ*, and *sir2RK* relative to WT on each of three chromosomes. Tetrad data upon which this analysis is based are given in Supplementary Table 2.

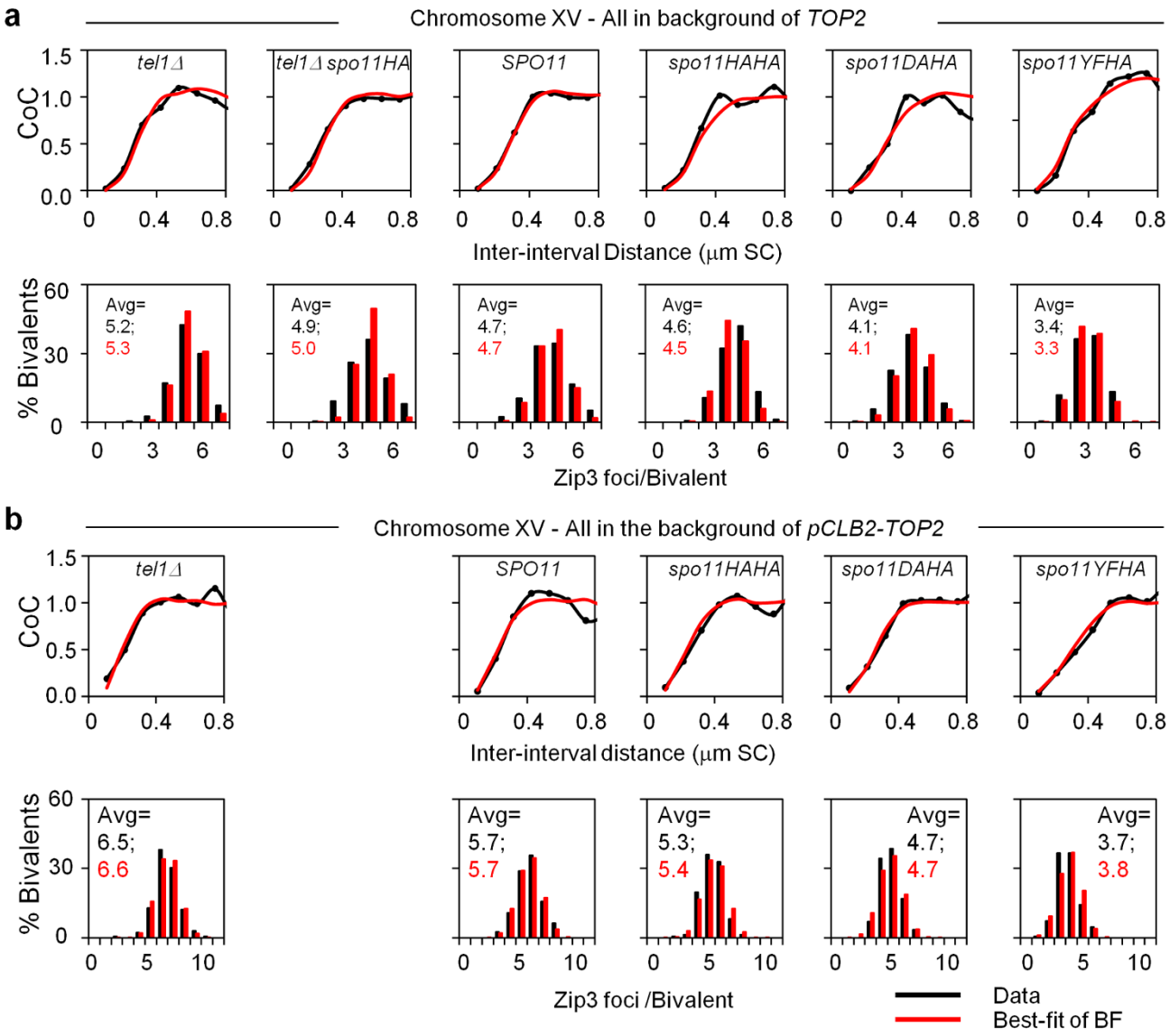

c Comparison of *rad50S* DSB levels and BF-predicted precursor levels (N) on chromosome XV

Strains	*tel1Δ*	*tel1Δ spo11HA*	*SPO11*	*spo11HAHA*	*spo11DAHA*	*spo11YFHA*
Relative DSB levels (*rad50S*)	150	120	100	80	70	30
DSBs per Chr XV	19	16	13	10.5	9.1	4
BF-predicted DSBs (precursors = (N))	19	16	13	11	10	7

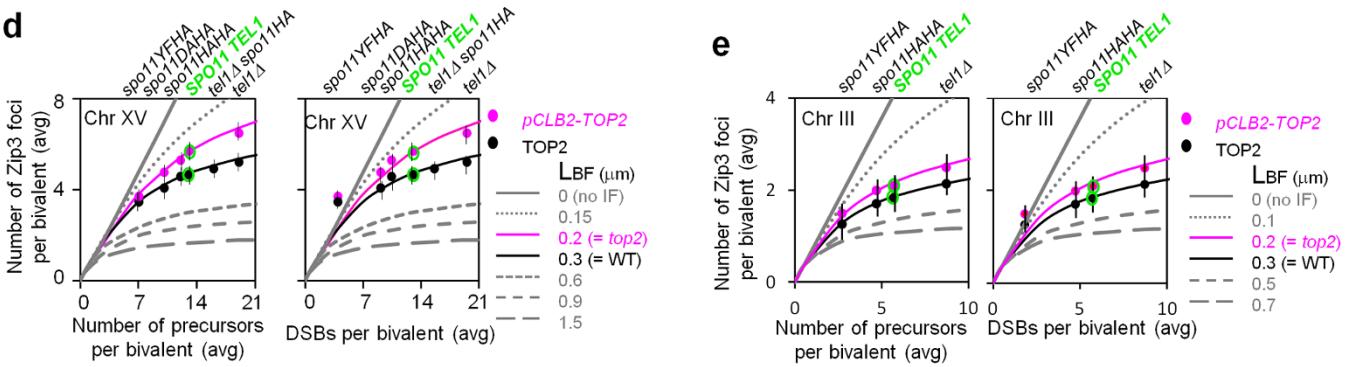

Extended Data Figure 4 | Additional aspects of crossover homeostasis analysis. **a**, **b**, Crossover patterns along chromosome XV in *TOP2* strains (**a**, black) and *pCLB2-TOP2* strains (**b**, black) with WT or altered DSB levels as conferred by the indicated *spo11/tel1* genotypes (for crossover homeostasis analysis; Fig. 2d and Methods). All experimental data sets were also subjected to beam-film simulation analysis (**a** and **b**, red). In all cases (**a** and **b**, red), best-fit simulations were obtained by using the same parameters as those that give the best-fit for *SPO11 TEL1* meiosis (ref. 8; Fig. 2a) except that number of precursors (given by parameter *N*) was altered to account for alterations in DSB levels in the different strain backgrounds (L_{BF} = 0.3 μm in *TOP2* background versus 0.2 μm in *PCLB2-TOP2* background; see Methods and below). For each *spo11/tel1* genotype, the best-fit value of (*N*) is the same in *pCLB2-TOP2* as in *TOP2*, thus confirming that the only change in various *pCLB2-TOP2* strains examined is a change in precursor number, with no change in interference. The same results are also seen for beam-film simulations of analogous data for chromosome III (not shown). These results further illustrate the accuracy with which beam-film simulations can describe diverse crossover patterns. **c**, Comparison of *rad50S* DSB levels and beam-film-predicted precursor levels (*N*) for chromosome XV among strains with varying DSB levels due to different *SPO11 TEL1* or carrying *spo11* and/or *tel1* mutant alleles. Top line: number of DSBs genome-wide, relative to WT = 100, as defined by *rad50S* analysis in *TOP2* strains, either *SPO11 TEL1* or carrying *spo11* and/or *tel1* mutant alleles (details in Methods). Middle line: number of DSBs predicted for chromosome XV. Number of DSBs in *TOP2 SPO11 TEL1* was defined by several approaches (details in Methods). DSBs per chromosome XV as predicted for *spo11/tel1* mutant strains by comparison of *rad50S* DSB levels with *SPO11 TEl1* (top line). Bottom line: number of precursors predicted to be present by beam-film best-fit simulation analysis (given by parameter *N*, above). Predicted values are the same for *TOP2* and *pCLB-TOP2* strain series (from simulations in **a** and **b**). Note that in strains with lower total DSB levels, *rad50S* analysis gives lower DSB/precursor levels than beam-film simulations (discussion in Methods). Analogous results are obtained for chromosome III, as follows. (1) The predicted values of *N* are the same for both *TOP2* and *pCLB2-TOP2* strain series: *N* = 9 for *tel1Δ*, 6 for *TEL1 SPO11*, 5 for *spo11-HA/spo11HA* and 3 for *spo11-HA/spo11YF*. (2) These predicted values of *N* correspond well to DSB values predicted from *rad50S* analysis except at the lowest DSB levels: predicted DSBs = 9 for *tel1Δ*, 6 for *TEL1 SPO11*, 5 for *spo11-HA/spo11HA* and 2 for *spo11-HA/spo11YF*. **d**, Experimentally determined numbers of Zip3 foci from the analyses of chromosome XV in **a** and **b** are plotted as a function of either the number of precursors predicted by beam-film simulation analysis (left) or the number of DSBs predicted by *rad50S* DSB analysis (right) (values from **c**). **e**, Same as **d**, except that we analysed chromosome III. A slightly better match of experimental data to beam-film simulation predictions is obtained when the *x* axis metric is the predicted precursor number than when it is *rad50S* predicted DSB levels, suggesting that beam-film simulations are more accurate than *rad50S* DSB analysis, which is known to underestimate DSBs in several situations. Note that for each strain and chromosome, Zip3 foci were analysed in 200–300 cells. The average numbers of foci per bivalent ± s.d. as presented in **d** and **e** were as follows. *TOP2* chromosome XV (**d**): *tel1Δ* 5.21 ± 0.93; *tel1Δ spo11HA* 4.92 ± 1.12; *TEL1 SPO11* 4.67 ± 1.16; *spo11HA/spo11HA* 4.11 ± 0.97; *spo11HA/spo1DA* 4.07 ± 1.07; *spo11HA/spo11YF* 3.51 ± 0.88. *pCLB2-TOP2* chromosome XV (**d**): *tel1Δ* 6.46 ± 1.13; *TEL1 SPO11* 5.96 ± 1.1; *spo11HA/spo11HA* 5.29 ± 0.99; *spo11HA/spo11DA* 4.76 ± 0.94; *spo11HA/spo11YF* 3.71 ± 0.98. *TOP2* chromosome III (**e**): *tel1Δ* 2.16 ± 0.59; *TEL1 SPO11* 1.82 ± 0.55; *spo11HA/spo11HA* 1.7 ± 0.62; *spo11HA/spo11YF* 1.31 ± 0.66. *pCLB2-TOP2* chromosome III (**e**): *tel1Δ* 2.49 ± 0.82; *TEL1 SPO11* 2.1 ± 0.87; *spo11HA/spo11HA* 2.07 ± 0.75; *spo11HA/spo11YF* 1.51 ± 0.69.

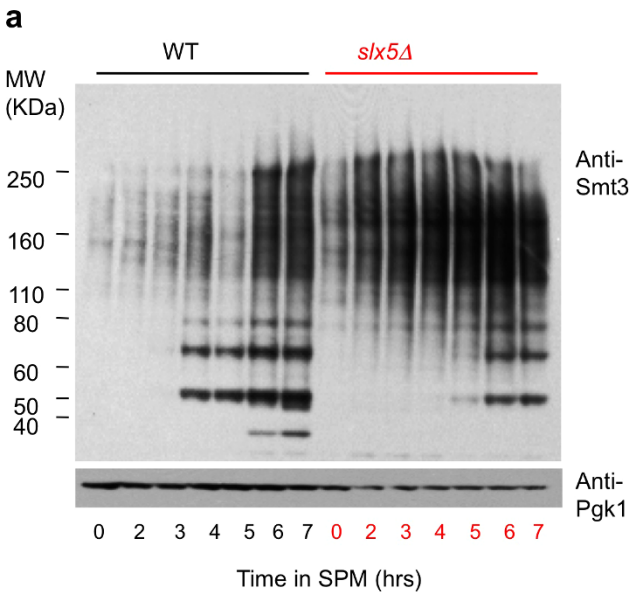

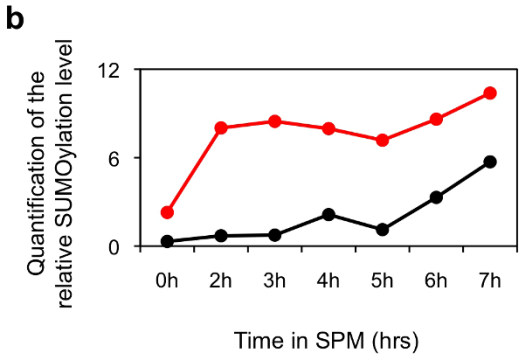

Extended Data Figure 5 | Increased level of SUMO–protein conjugates in *slx5Δ*. **a**, Western blots for whole protein extracts in WT and *slx5Δ* probed with anti-Smt3 antibody (Santa Cruz, sc-28649) and anti-Pgk1 antibody (Abcam ab113687) as a function of time after entry into meiosis ($t = 0$). Abundance of SUMO conjugates is increased in the mutant, especially in regions of high molecular mass. **b**, Quantification of the gel in **a**.

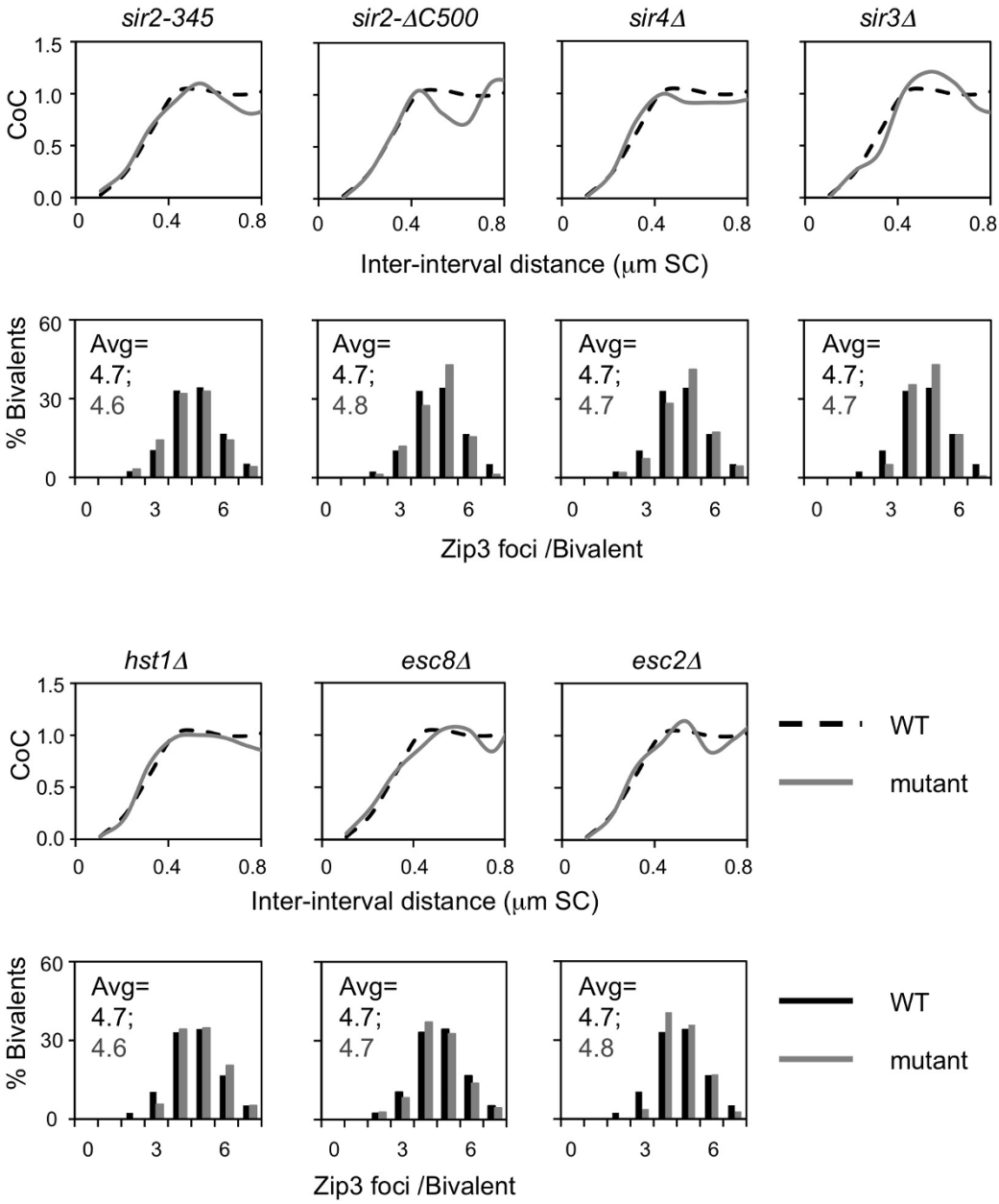

Extended Data Figure 6 | The role of Sir2 in crossover interference is specific to its interaction with Slx5. WT crossover interference is seen in diverse *sir2* non-null mutants affecting specific sub-functions (other than *sir2RK*; Fig. 3) and in mutants deleted for various interaction partners. *sir2-345* is defective in histone deacetylase activity[63]; *sir2ΔC500* lacks a Sir2 cohesion role[64]. *sir3Δ*, *sir4Δ*, *esc2Δ* and *esc8Δ* eliminate Sir2 interaction partners involved in silencing[43,65]; *hst1Δ* eliminates a Sir2 homologue[66].

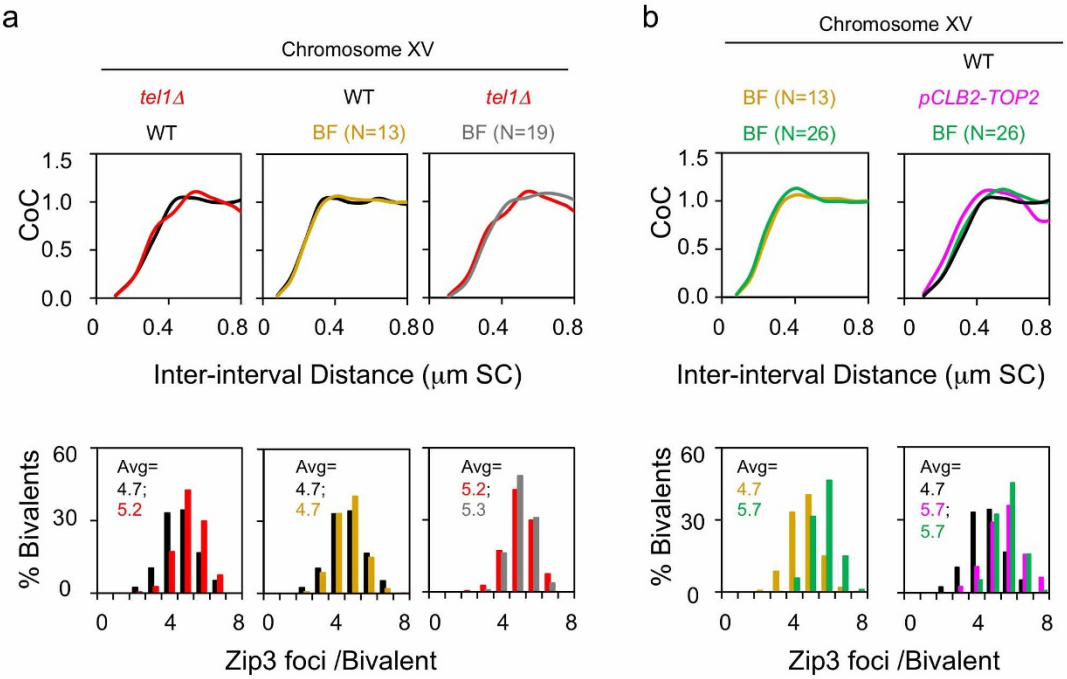

Extended Data Figure 7 | Mutant coefficient of coincidence and crossover number phenotypes cannot be explained by increased DSBs or by prolongation of the crossover-designation stage. Mutants in the described crossover interference pathway all confer coordinate changes in crossover interference, which is reduced, and the total number of crossovers, which is increased, by about 20% on chromosome XV. There are the expected consequences of a single defect in crossover interference, as illustrated by corresponding beam-film simulations, which quantitatively explain these results by a change in a single parameter, the interference length (L_{BF}) (Figs 2 and 3). This interference defect could comprise a defect in generation and spreading of the inhibitory signal and/or of the ability of unreacted precursors to respond to that signal (see text and Methods (section 'Beam-film simulations')). An increase in the number of crossovers can also occur as the result of either (1) prolongation of the crossover-designation period or (2) an increase in the number of DSBs[8]. Neither of these effects can explain the mutant phenotypes described in the text. (1) Crossover designation precedes synaptonemal complex formation and thus the pachytene stage[14]. Time-course analysis of representative mutant strains reveals that, in *sir2* mutants and in *top2SNM*, meiosis proceeds through pachytene and the two meiotic divisions normally (Extended Data Fig. 8a; ref. 14; data not shown). *slx5/8* mutants and *PCLB2-TOP2* mutants show no delay in progressing through prophase to pachytene (data not shown) but show a delay in meiosis I (*slx5*) or pachytene arrest (*PCLB2-TOP2*) (Extended Data Fig. 8a; data not shown). The *pCLB2-TOP2 top2YF* mutant does show a delay in achieving pachytene, as well as pachytene arrest, but exhibits the same crossover patterning phenotype as all other mutants, which show no pre-pachytene delay. Thus, prolonged crossover designation is not the basis for these phenotypes. (2) An increase in DSBs, without any change in crossover interference, does increase the number of crossovers; however, it has very little effect on crossover interference relationships (coefficient of coincidence curves) in budding yeast[8]. Correspondingly, two lines of evidence show that the mutant defects described here cannot be attributed to an increase in DSBs. **a**, A *tel1Δ* mutant exhibits increased DSBs but no change in coefficient of coincidence relationships. *TEL1* encodes the yeast homologue of ATM. Absence of Tel1 confers a 50% increase in DSBs[62] and a 10% increase in number of Zip3 foci (Supplementary Fig. 7 in ref. 8; reproduced in Extended Data Fig. 7a left, red colour). However, (1) there is no change in coefficient of coincidence relationships relative to WT (Extended Data Fig. 7a left), (2) the increase in crossovers is precisely that predicted on the basis of crossover homeostasis (ref. 8; text Fig. 2d, filled black circle at 19 DSBs/precursors per chromosome XV) and (3) beam-film simulation accurately describes the *tel1Δ* phenotype, relative to WT, by a change in a single parameter: the level of DSBs ($n = 19$, grey, versus 13, gold, in WT). The last point is documented in Extended Data Fig. 7a middle and right. The middle panel in Extended Data Fig. 7a shows the beam-film best-fit simulation for WT chromosome XV, where $n = 13$ (gold), compared with the experimental coefficient of coincidence curve (black; from Fig. 1); the right panel shows the beam-film best-fit simulation for *tel1Δ* chromosome XV, where $n = 19$ (grey) and all other parameters are the same as for WT, compared with the experimental coefficient of coincidence curve (red) from the left panel. **b**, Beam-film simulations predict no/little change in coefficient of coincidence with increasing DSBs for yeast chromosome XV (data not shown). More specifically, to explain the increased number of crossovers observed in the analysed mutants, for example *pCLB2-TOP2*, the value of N required for beam-film simulations of chromosome XV would be 26 (double the WT value of $N = 13$). If beam-film simulations are performed under the same parameter values used for WT except that $N = 26$ instead of $N = 13$, the predicted coefficient of coincidence curve is unchanged compared with that predicted for WT (left panel, compare gold for $N = 13$ with green for $N = 26$). Correspondingly, the coefficient of coincidence curve predicted for $N = 26$ (green) matches the WT coefficient of coincidence curve (black) and is unlike the coefficient of coincidence curve for the mutant (pink) (right panel). Additional evidence that DSB number is not altered in *pCLB2-TOP2* versus *TOP2* is presented in Extended Data Figs 4 and 8.

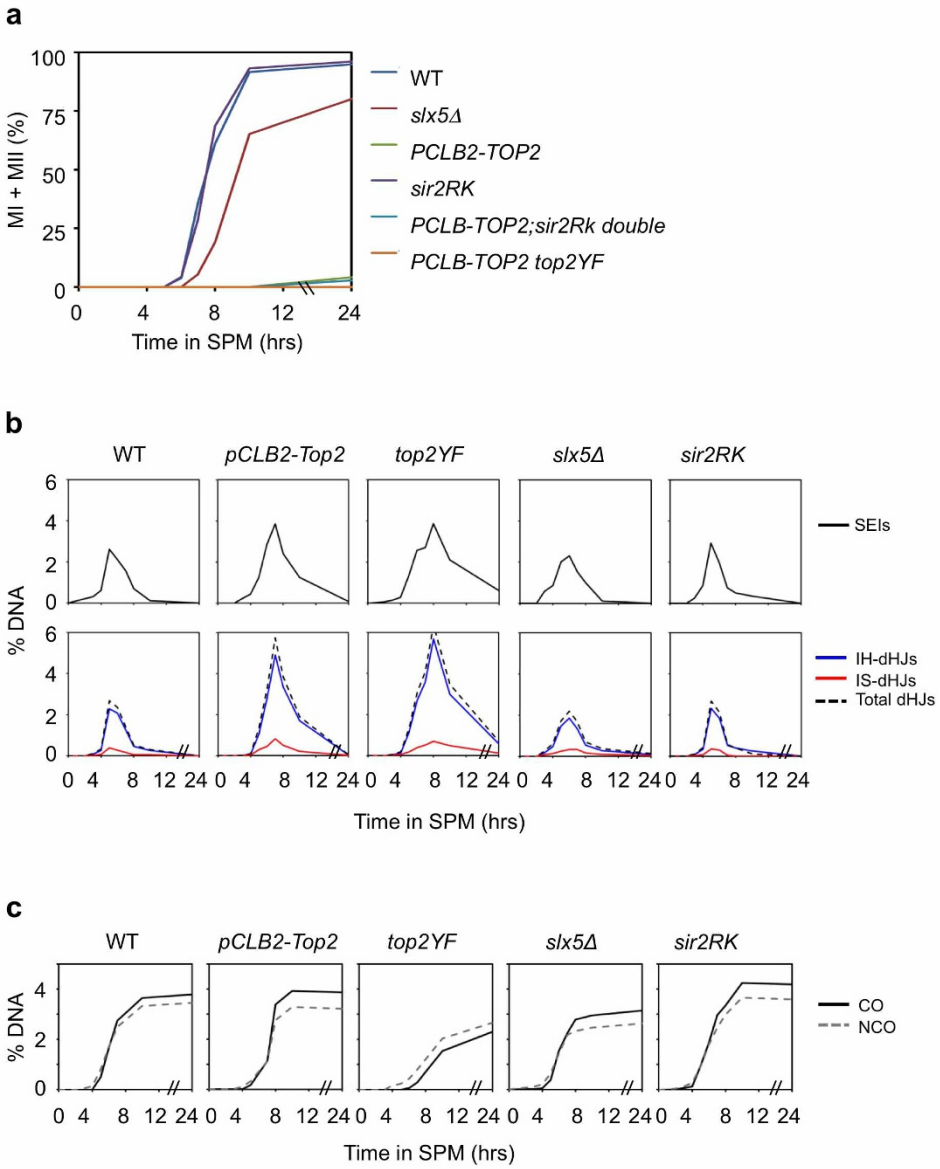

Extended Data Figure 8 | Progression of meiosis and of recombination in interference-defective mutants. Representative mutants were examined for progression of meiotic divisions and for recombination at the previously characterized *HIS4LEU2* locus[67] (strains in Extended Data Table 1). **a**, Meiotic divisions. The first meiotic division occurs normally in *sir2RK* (defective in interaction with Slx5); it is delayed in *slx5Δ* and is completely absent in *PCLB2-TOP2* and *PCLB-TOP2 top2YF* due to arrest at pachytene[23] (L.Z., unpublished observations). **b**, **c**, DNA events. The *HIS4LEU2* locus probably provides a direct readout of DNA events independent of the effects of interference. *HIS4LEU2* does not exhibit crossover homeostasis[24], which implies that it is not sensitive to crossover interference[8]. This feature presumably reflects the fact that this locus is a very strong DSB hot spot. A DSB occurs at this site in virtually every nucleus with a concomitant reduction in DSBs (and thus crossover precursors) at other positions in its vicinity (N.K., unpublished observations). This locus may also undergo early crossover designation, thus also dominating crossover interference patterns per se. Importantly, Zip3 foci are used for diagnosis of crossover interference relationships[8]. Zip3 foci form as a specific consequence of programmed crossover designation; they do not mark the sites of non-interfering crossovers, which exhibit an entirely different pattern along the chromosomes[8]. Furthermore, formation of Zip3 foci is upstream of, and thus insensitive to, defects in later events, including (1) major perturbations in the kinetics of recombination or the fidelity with which initiated events (crossover-fated and/or non-crossover-fated) proceed to their assigned fates (see, for example, ref. 14) or (2) the potential occurrence of additional DSBs due to delayed synaptonemal complex formation (discussion in refs 8 and 56). Thus, none of the recombination aberrancies detected by physical analysis of recombination in the analysed mutants (below) is relevant to their crossover interference phenotypes. Correspondingly, although all mutants give exactly the same crossover patterns (interference and crossover number) as defined by Zip3 foci, the mutants vary widely with respect to DNA recombination phenotypes. The results below can be summarized to say that (1) absence of Slx5/8-Sir2 STUbL activity has little, or only subtle, effect(s) on recombination, whereas (2) absence of TopoII or TopoII catalytic activity confers delays and aberrancies. **b**, DSBs, SEIs and dHJs. Progression through recombination is very similar to WT in *sir2RK* and *slx5Δ*. Both *PCLB2-TOP2* and *PCLB-TOP2 top2YF* exhibit a phenotype corresponding to delayed progression beyond the point of crossover designation: DSBs appear on time; however, DSBs, single-end invasions (SEIs) and double Holliday junctions (dHJs) all accumulate to higher than normal levels at later than normal times, implying delayed progression of crossover-designated DSBs to SEIs, and of SEIs to dHJs, where SEIs and dHJs are both crossover-specific intermediates[14]. There is no significant alteration in homologue-versus-sister bias in any of the four mutants, with inter-homologue dHJs predominating over inter-sister dHJs similarly to WT in all cases. **c**, Inter-homologue crossover (CO) and non-crossover (NCO) products. Inter-homologue crossover and non-crossover levels are very similar to WT in *PCLB2-TOP2* and show variations relative to WT in the other mutants. A differential deficit of crossovers versus non-crossovers in *PCLB2-TOP2 top2YF* suggests a specific defect in crossover maturation in this mutant.

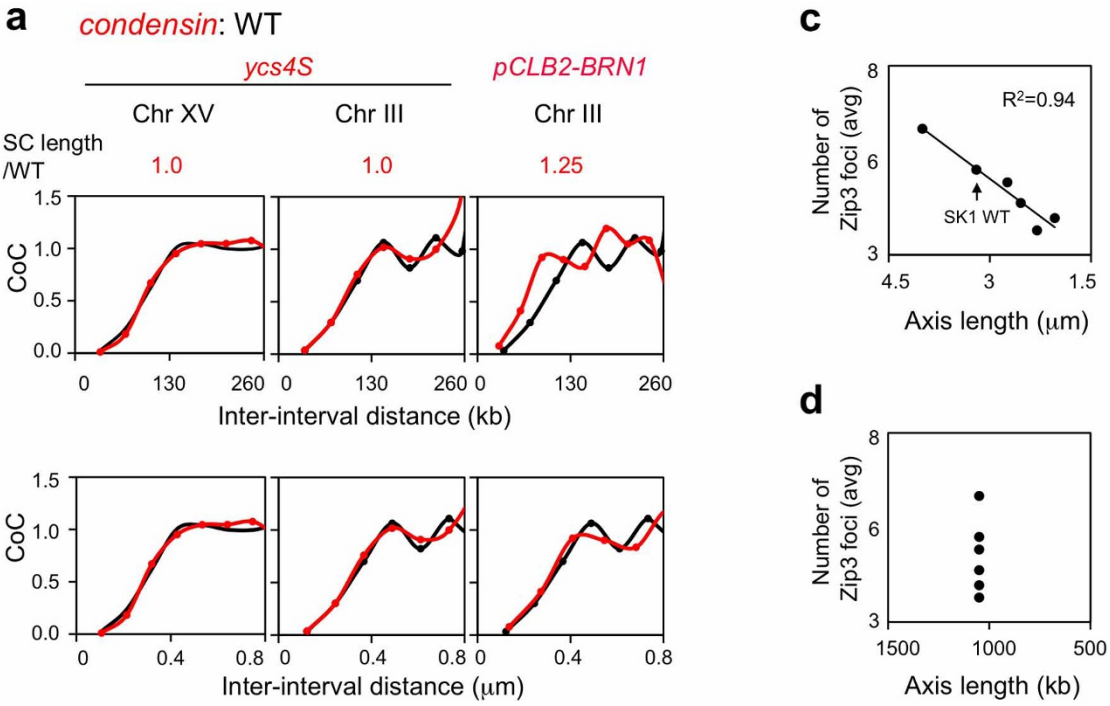

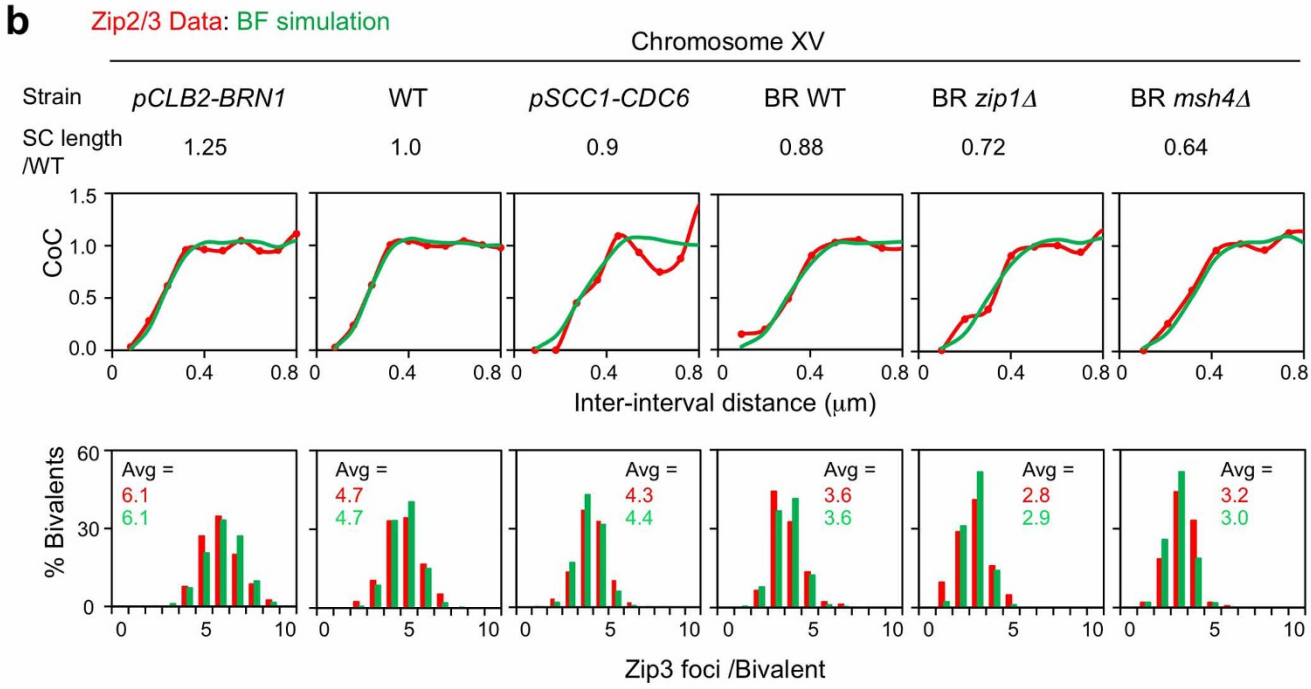

Extended Data Figure 9 | The metric of crossover interference is physical axis length (micrometres). **a**, This study considered two different condensin mutants, *ycs4S* and *pCLB2-BRN1*. Axis length is normal in *ycs4S* and longer than normal in *pCLB2-BRN1*. Analysis presented for chromosome XV in *pCLB2-BRN1* (Fig. 5) was also done on chromosome III in that mutant background (right column), confirming that coefficient of coincidence relationships are WT when the metric is physical chromosome length but not when the metric is genomic distance. We similarly analysed chromosomes III and XV in the *ycs4S* background (left and middle columns), confirming WT coefficient of coincidence relationships by both metrics. **b**, Zip3 focus analysis for chromosome XV in the indicated strains (red; from Fig. 5) and beam-film simulation analysis (green). Best-fit simulations could be obtained for all strains using the same parameter values as for WT meiosis, including interference distance ($L_{BF} \approx 0.3$ μm), except that the number of precursors (N) had to be varied linearly with axis length. For the indicted strains, from left to right, $N = 17, 13, 12, 10, 9$ and 8. This result implies direct interplay between physical chromosome length (micrometres of synaptonemal complex) and DSB probability, as discussed elsewhere. **c**, **d**, For the mutant cases described in **b**, experimentally observed average numbers of Zip3 foci vary linearly with axis length (**c**). In contrast, different numbers of Zip3 foci are observed for the different strains despite the fact that chromosome XV has the same genomic length in all cases (**d**). We also note that the best fit simulation for BR *zip1Δ* had to include a 10% decrease in the 'efficiency of maturation of crossover-designated interactions', which, in the present context, implies that in a *zip1Δ* background there is a 10% reduction in either (1) the stability of a Zip3 focus under cytological spreading conditions at the absence of synaptonemal complex or (2) the probability that a crossover designation will give a Zip3 focus.

Extended Data Table 1 | Strains used in this study

Strains	Genotype
NKY4146	*HMR::LacO-URA3/", URA3::CYC1p-LacI-GFP/", ZIP3-13myc::Hygromycin*
NKY4147	*URA3::CYC1p-LacI-GFP/", scp1(Ch XV telomere)::LacO-LEU2/", ZIP3-13myc::Hygromycin*
NKY4148	*leu2::LacI-GFP::Clonat/", tel4::226xLacO::Kan/", ZIP3-13myc::Hygromycin*
LZY1842	as NKY4146, except *pCLB2-TOP2:KanMX/"*
LZY1570	as NKY4147, except *pCLB2-TOP2:KanMX/"*
LZY1845	as NKY4148, except *pCLB2-TOP2:KanMX/"*
LZY2306	as NKY4147, except *top2-SNM::KanMX/"*
LZY2190	as NKY4147, except *pCLB2-TOP2:KanMX/", top2(Y782F):URA3*
LZY2237	as NKY4147, except *ubc9-GFP::KanMX/"*
LZY2207	as NKY4147, except *red1::kanMX6/", LEU2::pYI-red1KR*
LZY2262	as NKY4147, except *pCLB2-TOP2:KanMX/", tel1D::KanMX/"*
LZY2194	as NKY4147, except *pCLB2-TOP2:KanMX/", spo11-HA3His6::KanMX4/"*
LZY2187	as NKY4147, except *pCLB2-TOP2:KanMX/", spo11-HA3His6::KanMX4/spo11(D290A)-HA3His6::KAnMX4*
LZY2266	as NKY4147, except *pCLB2-TOP2:KanMX/", spo11-HA3His6::KanMX4/spo11-(Y135F)-HA3His6::KanMX*
LZY2054	as NKY4147, except *slx5D::natMX/"*
LZY2418	as NKY4148, except *slx5D::natMX/"*
LZY1983	as NKY4147, except as *slx8D::natMX/"*
LZY2325	as NKY4147, except *slx5D::nat1::slx5-sim(1-4)::KanMX/"*
LZY2319	as NKY4147, except *slx8-SS::natMX/"*
LZY1572	as NKY4147, except *sir2D:KanMX/"*
LZY1667	as NKY4146, except *sir2D:KanMX/"*
LZY2166	as NKY4148, except *sir2D:KanMX/"*
LZY2012	as NKY4147, except *sir2D::KanMX4::Sir2-R139K::natMX/"*
LZY1756	as NKY4147, except *sir2-345:: natMX/"*
LZY1702	as NKY4147, except *sir2-DC500::KanMX/sir2-DC500::natNT2*
LZY1516	as NKY4147, except *sir3D::LEU2/"*
LZY1723	as NKY4147, except *sir4D::KanMX/sir4::natNT2*
LZY2146	as NKY4147, except *esc2D::KanMX/"*
LZY1718	as NKY4147, except *esc8D::KanMX/"*
LZY1451	as NKY4147, except *hst1D::KanMX/"*
LZY1201	as NKY4147, except *ndj1D::KanMX/"*
LZY1446	as NKY4147, except *hta1-S128A/", hta2-S128A/"*
LZY1986	as NKY4147, except *pCLB2-NSE2::KanMX/"*
LZY932	as NKY4147, except *dot1D::KanMX/"*
LZY2006	as NKY4147, except *smc6-9::NAT/"*
LZY1163	as NKY4147, except *ndt80D::LEU2/", REC8-3HA::URA3/+, pCLB2BRN1::KANMX4/"*
LZY1325	as NKY4146, except *ndt80D::LEU2/", REC8-3HA::URA3/+, pCLB2BRN1::KANMX4/"*
LZY1261	as NKY4147, except *ndt80D::KanMX/", REC8-3HA::URA3/+, ycs4S/"*
LZY1364	as NKY4146, except *ndt80D::KanMX/", REC8-3HA::URA3/+, ycs4S/"*
LZY1471	as NKY4146, except *pch2D::KanMX/"*
LZY1488	as NKY4148, except *pch2D::KanMX/"*
LZY1472	as NKY4147, except *pch2D::KanMX/"*
LZY773	as NKY4147, except *cdc6::kanMX6::PSCC1:3-HA-CDC6/", ndt80::LEU2/"*
LZY1317	as NKY4147, except *mlh1D::KanMX/"*
LZY1386	as NKY4147, except *mlh3D::KanMX/"*
LZY1318	as NKY4147, except *mms4D::KanMX/"*
LZY1504	as NKY4147, except *msh2::LEU2/"*
LZY2018	as NKY4147, except *sir2D::KanMX4::Sir2-R139K::nat/", pCLB2-TOP2::KanMX/"*
LZY2080	as NKY4147, except *sir2D::KanMX4::Sir2-R139K::nat/", slx5D::natMX/"*
LZY2313	as NKY4147, except *slx5D::natMX/", red1::kanMX6/", LEU2::pYI-red1KR,*
LZY2430	as NKY4147, except *slx5D::natMX/", top2-SNM::KanMX/"*
LZY2341	as NKY4147, except *top2-SNM::KanMX, red1::KanMX, LEU2-red1KR*
LZY446	*ho::hisG leu2 ura3 nuc1::hygroB HIS4::LEU2-(BamHI+ori), MAT alpha*
LZY447	*ho::hisG leu2 ura3 nuc1::hygroB his4-x::LEU2-(NgoMIV+ori)--URA3, MAT a*
LZY1614	as LZY446, except *pCLB2-TOP2::KanMX*
LZY1617	as LZY447, except *pCLB2-TOP2::KanMX*
LZY2413	as LZY446, except *pCLB2-TOP2::KanMX, URA3::top2(Y782F)*
LZY2414	as LZY447, except *pCLB2-TOP2::KanMX, URA3::top2(Y782F)*
LZY2261	as LZY446, except *slx5D::natMX*
LZY2255	as LZY447, except *slx5D::natMX*
LZY2198	as LZY447, except *sir2D::KanMX4::Sir2-R139K::nat*
LZY2199	as LZY447, except *sir2D::KanMX4::Sir2-R139K::nat*

All strains are isogenic derivatives of SK1 with *ho::hisG*, *leu2* and *ura3*.